Department of Physics and Astronomy

University of Heidelberg

Master's thesis in Physics

submitted by

Kathrin Kromer

born in Freiburg im Breisgau (Germany)

2019

Environmentally-induced systematic effects at the high-precision mass spectrometer PENTATRAP

This master's thesis has been carried out by Kathrin Kromer
at the Max Planck Institute for Nuclear Physics in Heidelberg
under the supervision of Prof. Dr. Klaus Blaum

Systematische Effekte durch Umwelteinflüsse am Hochpräzisions-Massenspektrometer PENTATRAP

PENTATRAP ist ein Massenspektrometer, das aus fünf Penning-Fallen besteht. Es dient zur Messung des Massenverhältnisses langlebiger, hochgeladener Ionen mit einer relativen Genauigkeit von unter 10^{-11}, welche erzielt wird indem die Zyklotronfrequenzen von gespeicherter Ionen in einem starken Magnetfeld bestimmt werden. Massenverhältnisse, die so präzise bestimmt werden, können unter anderem einen Beitrag zur Neutrinophysik und zu einem direkten Test der speziellen Relativitätstheorie leisten. Um dieses Ziel zu erreichen, müssen die systematischen Fehler der Zyklotronfrequenzmessung durch Umwelteinflüsse, wie Magnetfeld-, Druck- und Temperaturschwankungen, genau bekannt sein und vermieden werden.
Im Rahmen dieser Arbeit wurden die Hauptursachen für Magnetfeldänderungen identifiziert und es wurde ein aktives Magnetfeldstabilisierungssystem konstruiert und getestet. Die Temperatur im Labor wurde auf eine Stabilität von 20 mK/h optimiert und die Temperaturabhängigkeit der Spannungsquelle für die Fallenpotentiale auf $2{,}43(14) \cdot 10^{-6}$/K und weniger bestimmt. Es wurde ein System installiert und erfolgreich getestet, das das Heliumlevel und den Druck in der Bohrung des Magneten stabilisiert. Das Stabilisierungssystem hat die Fluktuationen des magnetischen Feldes in der Falle auf einen nahezu konstanten, relativen Drift von $-2 \cdot 10^{-10}$/h reduziert. Mit der erreichten Kontrolle über die Umwelteinflüsse wurden die ersten Zyklotronfrequenzmessungen von ^{187}Re/^{187}Re, mit einer relativen Genauigkeit von $8 \cdot 10^{-12}$, durchgeführt.

Environmentally-induced systematic effects at the high-precision mass spectrometer PENTATRAP

PENTATRAP is a mass spectrometer consisting of five Penning traps aiming for mass-ratio measurements of long-lived, highly-charged ions to a relative precision of below 10^{-11} by determining the cyclotron frequencies of trapped ions in a strong magnetic field. At this level of precision, mass-ratio determinations contribute, among others, to neutrino physics and a direct test of special relativity. In order to reach this goal, the systematic uncertainties of the cyclotron frequency measurement originating from environmental influences, including magnetic field, pressure, and temperature fluctuations, have to be precisely known and avoided.
In the framework of this thesis, the main sources of magnetic field changes have been identified and an active magnetic field stabilization system was constructed and tested. The temperature was optimized to a stability of 20 mK/h and the temperature dependence of the voltage source for the trapping potentials of the measurement traps was determined to be $2.43(14) \cdot 10^{-6}$/K and less. A helium-level and cold-bore pressure stabilization system has been installed and successfully tested, reducing the fluctuations of the magnetic trapping field to a nearly constant relative drift of $-2 \cdot 10^{-10}$/h. With the achieved control over the environmental influences the first cyclotron frequency measurements of ^{187}Re/^{187}Re to a relative precision of $8 \cdot 10^{-12}$ have been carried out.

Contents

List of Figures

List of Tables

Chapter 1

Introduction

High-precision mass spectrometry plays a prominent role in many fields of physics and can be used, e.g. to test predictions of fundamental theories. One of these theories is Einstein's special relativity with its famous equation: $E = mc^2$ [Rain 04]. This mass-energy equivalence has been tested to hold to a level of at least 0.00004% by comparing the atomic-mass difference Δm of the silicon isotopes ^{28}Si and ^{29}Si and the sulphur isotopes ^{32}S and ^{33}S, multiplied by the speed of light c squared, to the γ-ray energy in the neutron capture process of ^{28}Si and ^{32}S [Rain 05]. In this experiment the mass difference on one side of the equation was determined by measuring cyclotron frequency ratios, which are inversely proportional to the mass ratios, of two simultaneously stored ions in a Penning trap [Rain 04]. For the other side of the equation, the energy of the γ-rays emitted during the neutron capture of ^{28}Si and ^{32}S, creating ^{29}Si and ^{33}S, were measured by the GAMS4 crystal-diffraction facility at the Institut Laue-Langevin (*ILL*) in Grenoble [Kess 01]. The neutron-capture process:

$$^{A}\mathrm{X} +^{1}_{0}\mathrm{n} \rightarrow^{A+1} \mathrm{X}^{*} \rightarrow^{A+1} \mathrm{X} + \gamma \tag{1.1}$$

releases the binding energy of the captured neutron via an emission of γ-rays. Using crystal Bragg spectroscopy, the wavelength λ and thereby the energy $E = \frac{hc}{\lambda} = h\nu$, with the Planck constant h, of the emitted γ-rays are measured and summed up to determine the total energy released during the neutron-capture process. For testing the mass-energy equivalence, the mass-difference and the γ-ray energy have been combined in the following way [Rain 05]:

$$\Delta mc^2 = (m[^{A}\mathrm{X}] - m[^{A+1}\mathrm{X}] - (m[\mathrm{D}] - m[\mathrm{H}]))c^2 = h(\nu_{A+1} - \nu_D) \ , \tag{1.2}$$

with the γ-ray frequency ν_{A+1}, the neutron mass determined by the mass difference of deuterium m(D) and hydrogen m(H), and the frequency corresponding to the deuterium binding energy ν_D. The resulting agreement of $1 - \Delta mc^2/E = (-1.4 \pm 4.4) \cdot 10^{-7}$ with the mass-energy equivalence has been the most precise test of Einstein's famous equation so far. The limiting factor on the experiment's precision was the measurement of the diffraction angles of the highest-energy γ-rays. The fractional accuracy of these diffraction angles was about 10^{-7} [Rain 05].

In order to improve the precision of this test of special relativity, PENTATRAP is planning to measure the mass difference of ^{35}Cl and ^{36}Cl. The precision of the γ-ray spectroscopy will be improved due to the higher neutron capture cross section of ^{35}Cl of 43.63 b since a higher count count rate will lower the statistical uncertainty [NNDC]. By way of comparison, see neutron capture cross section of ^{28}Si: 0.1691 b and of ^{32}S: 0.5283 b. In addition to this, the new generation of the crystal-diffraction experiment at the ILL, GAMS6, is expected to reach a relative uncertainty of 10^{-8} of the γ-ray energies[Krem 10]. A proposal for this combined measurement has been accepted by the ILL.

For the determination of the mass difference of ^{35}Cl and ^{36}Cl, the absolute mass of ^{35}Cl has to be measured to highest precision. The mass ratio of ^{35}Cl will be measured as a ratio to the mass of ^{28}Si, which has been determined to a relative uncertainty of $1.8 \cdot 10^{-11}$ [Huan 17]. The mass difference can then be calculated from the measurement of two mass ratios: $R_{35\mathrm{Cl}/28\mathrm{Si}}$ and $R_{36\mathrm{Cl}/35\mathrm{Cl}}$ by:

$$\begin{aligned}\Delta m &= m[^{36}\mathrm{Cl}] - m[^{35}\mathrm{Cl}] = m[^{35}\mathrm{Cl}] \cdot \left(\frac{m[^{36}\mathrm{Cl}]}{m[^{35}\mathrm{Cl}]} - 1\right) \\ &= m[^{35}\mathrm{Cl}] \cdot (R_{36\mathrm{Cl}/35\mathrm{Cl}} - 1) = \left(\frac{m[^{35}\mathrm{Cl}]}{m[^{28}\mathrm{Si}]}\right) \cdot m[^{28}\mathrm{Si}] \cdot (R_{36\mathrm{Cl}/35\mathrm{Cl}} - 1) \\ &= R_{35\mathrm{Cl}/28\mathrm{Si}} \cdot m[^{28}\mathrm{Si}] \cdot (R_{36\mathrm{Cl}/35\mathrm{Cl}} - 1) \ . \end{aligned} \tag{1.3}$$

To reach the goal of a test of $E = mc^2$ to a relative precision of 10^{-8}, which the γ-ray measurement is planning to achieve, the mass ratios will have to be measured to a precision of $2.5 \cdot 10^{-12}$ [Repp 15]. This would be the most precise measurement of a mass ratio to date. In order to measure mass ratios to such a high precision, an advanced experimental setup to overcome current limitations on existing Penning-trap mass spectrometers is required. PENTATRAP with its unique combination of access to highly-charged ions, its highly-stable 7-T superconducting magnet, and a stack of five Penning traps equipped with single-ion sensitivity and non-destructive detection systems, is aiming for this high precision. Currently, the experiment allows routine mass-ratio measurements of relative uncertainties down to 10^{-11} [Risc 18]. However, in order to reach beyond that precision, presently limiting sources of systematic errors have to be investigated and, if possible, eliminated. During the framework of this thesis, the environmentally-induced systematic effects on the setup have been studied and stabilization systems for environmental parameters have been tested.

The thesis will have the following structure. Chap. 2 will give an introduction into the physics behind a Penning trap and the detection methods. Chap. 3 three will then describe the different sections of the experimental setup of PENTATRAP, closing with the environmental sensors installed around the laboratory. Chap. 4 will examine the systematic uncertainties on the cyclotron frequency determination originating from environmental influences and determine if a stabilization of the environmental parameters will be necessary. This leads over to Chap. 5, where the stabilization systems of these environmental parameters are introduced and the achieved stability will be described. Chap. 6 gives a summary and a short outlook.

Chapter 2

Basics of Penning traps

This chapter will give an introduction to the physics behind a Penning trap starting with the ideal trap and then continuing with the real trap, ion manipulation and lastly detection and frequency measurements. It will mostly cover the information necessary to understand this thesis (for a wider description see [Brow 86]). Penning traps are being used in several fields of physics including high-precision mass measurements due to their long storage times under well-defined conditions. The way Penning traps store ions is central to the understanding of our measurement principles and the influences the environment could have on the measured frequencies.

2.1 Ion motion in an ideal Penning trap

A Penning trap in the field of high-precision mass measurements aims to connect an ion mass determination to a frequency measurement. This connection is made by using a strong homogeneous magnetic field $\vec{B} = B\vec{e}_z$ for radial confinement of the ion. Adding an electric field $\vec{E}$ in z-direction results in the Lorentz force

$$\vec{F}_L = q(\vec{E} + \vec{v} \times \vec{B}) \ , \tag{2.1}$$

with q being the charge of the ion and $\vec{v}$ its velocity. In a pure magnetic field the ion oscillates with the so-called free-space cyclotron frequency:

$$\omega_c = \frac{q}{m}B \ . \tag{2.2}$$

To practically indefinitely elongate the storage time, making a highly precise frequency measurement possible, a confinement in axial direction is added by superimposing a weak electrostatic quadrupole potential

$$\Phi(z,\rho) = \frac{V_0}{2d^2}(z^2 - \frac{x^2+y^2}{2}) = \frac{V_0}{2d^2}(z^2 - \frac{1}{2}\rho^2) \ , \tag{2.3}$$

exploiting the electric field part of the Lorentz force. The potential is defined by the voltage V_0, the geometrical factor d characterizing the dimension of the trap, and x and ρ as axial and radial coordinates, respectively. For details see Fig. 2.1(a). The equations of motion follow from the Lorentz force (Eq. (2.1)):

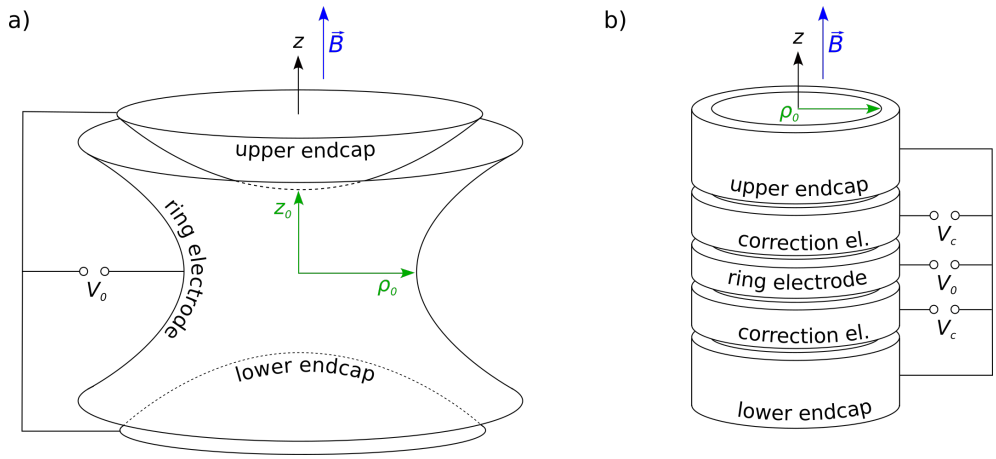

Figure 2.1: Comparison between a Penning trap with a) hyperbolic shaped electrodes and b) cylindrically shaped electrodes.

$$\begin{pmatrix} \ddot{x} \\ \ddot{y} \\ \ddot{z} \end{pmatrix} = \frac{qV_0}{2d^2} \begin{pmatrix} x \\ y \\ -2z \end{pmatrix} + \frac{qB}{m} \begin{pmatrix} \dot{y} \\ -\dot{x} \\ 0 \end{pmatrix} \tag{2.4}$$

For a full description of the derivation hereof and the following formulae see [Brow 86]. With the cylindrical symmetry of a Penning trap this leads to the following solutions featuring three independent eigenmotions with the eigenfrequencies ω_+, ω_-, ω_z, amplitudes ρ_+, ρ_-, ρ_z, and phases ϕ_+, ϕ_-, ϕ_z:

$$\begin{pmatrix} x(t) \\ y(t) \\ z(t) \end{pmatrix} = \rho_+ \begin{pmatrix} \sin\omega_+ t + \phi_+ \\ \cos\omega_+ t + \phi_+ \\ 0 \end{pmatrix} + \rho_- \begin{pmatrix} \sin\omega_- t + \phi_- \\ \cos\omega_- t + \phi_- \\ 0 \end{pmatrix} + \rho_z \begin{pmatrix} 0 \\ 0 \\ \sin\omega_z t + \phi_z \end{pmatrix} . \tag{2.5}$$

The radial motion is made up of a modified cyclotron motion with frequency ω_+ (which is the free-space cyclotron frequency with a correction from the electrostatic field) and a magnetron motion around the trap center with frequency ω_-:

$$\omega_\pm = \frac{\omega_c}{2} \pm \sqrt{\frac{\omega_c^2}{4} - \frac{\omega_z^2}{2}} . \tag{2.6}$$

In the axial direction a motion independent of the magnetic field takes place with the frequency

$$\omega_z = \sqrt{\frac{qV_0}{d^2 m}} . \tag{2.7}$$

These three independent eigenmotions add up to the complete motion of the ion. Fig. 2.2 shows an example of the individual motions as well as a trajectory of the superposition (dashed line). As a

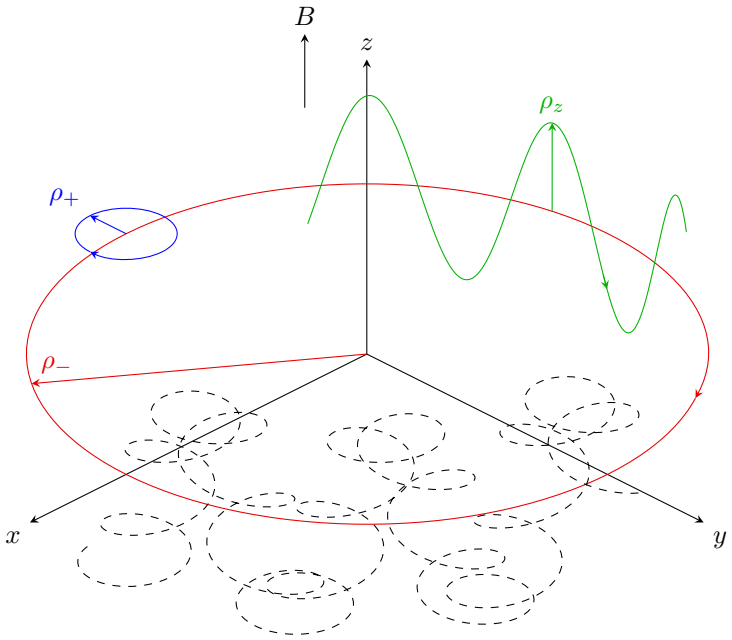

Figure 2.2: The figure shows the three eigenmotions of the stored ion: the modified cyclotron motion (blue line), the magnetron motion (red line), and the axial motion (green line). The dashed line represents the superposition of the three motions (trajectory of the ion).

trapping condition follows from Eq. (2.6):

$$\frac{\omega_c}{\sqrt{2}} > \omega_z \ . \tag{2.8}$$

The free-space cyclotron frequency can be calculated from Eq. (2.6) as

$$\omega_c = \omega_+ + \omega_- \tag{2.9}$$

or

$$\omega_c^2 = \omega_+^2 + \omega_-^2 + \omega_z^2 \ , \tag{2.10}$$

the second equation being called Brown-Gabrielse invariance theorem [Brow 86]. The frequency hierarchy results as:

$$\omega_c > \omega_+ > \omega_z > \omega_- \ . \tag{2.11}$$

2.2 Real Penning trap

The description of the real Penning trap takes small imperfections in the real Penning-trap experiment into consideration. Among these are the anharmonic part of the electric field and the inhomogenous part of the magnetic field, which will be briefly described in the following sections. Another unavoidable imperfection is the misalignment of the electrodes among themselves and in comparison to the magnetic

field axis. As described in [Brow 86] these small misalignments can be disregarded due to the validity of the invariance theorem, Eq. (2.10), even with the real frequencies $\bar{\omega}_{+,-,z}$, since the shifts cancel each other out

$$\omega_c^2 = \bar{\omega}_+^2 + \bar{\omega}_-^2 + \bar{\omega}_z^2 \ . \tag{2.12}$$

2.2.1 Electric field imperfections

A harmonic potential in Penning traps can be formed by using electrodes shaped like hyperboloids of revolution, see part of Fig. 2.1. At PENTATRAP, however, the traps have a cylindrical shape, which is a very common variation of the trap setup, since the larger opening signifies an easier injection of the ions and better vacuum pumping (motivation for cylindrical trap geometry see [Roux 12]). If additional correction electrodes are being fit in between the end caps and the ring electrode (see Fig. 2.1), an electric quadrupole potential can be approximated. The relation between the correction voltages V_c and the trapping voltage V_0 requires the theoretical determination of the optimal tuning ratio $TR = \frac{V_c}{V_0}$, which best approximates a harmonic potential (For PENTATRAP this is described in detail in [Roux 12]).
The electrode configurations shown in Fig. 2.1 give an idea of the origin of the anharmonic part of the electric field, including finite size of the electrodes, surface quality, a necessary hole in the hyperbolic-shaped electrodes for the ions to enter the trap and an imperfectly harmonic potential in the case of a cylindrical geometry. Using Legendre polynomials P_k and spherical coordinates the series

$$\Delta V(\rho, \theta) = \frac{1}{2} V_0 \sum_{k=1}^{\infty} C_k \left(\frac{\rho}{d}\right)^k P_k(cos\theta) \tag{2.13}$$

describes the potential difference to the ideal harmonic potential around the trap center. C_k are the strengths of the contributions of different orders. Since Penning traps are symmetric under $z \rightarrow -z$ transformation, all uneven orders in k in the series disappear [Kett 14]. The second order correction $k = 2$ shifts ω_z by a linear term, however, it shifts ω_+ and ω_- which depend on ω_z as well and with opposite signs, leaving the sum frequency ω_c unchanged. As leading orders remain $k = 4$ and 6 for the correction of the cyclotron frequency.

2.2.2 Magnetic field imperfections

The strong superconducting magnets used in Penning-trap experiments have a nearly homogeneous field at the center. However, for larger radii the ions might probe slightly inhomogeneous magnetic fields. Especially in a setup like PENTATRAP, which uses several traps at different positions in the magnetic field, the inhomogeneities of the field have to be taken into account. When lowering the trap into the cold bore of the superconducting magnet, it adds more magnetically susceptible material, thereby locally deforming the magnetic field lines which can change the frequencies of the ions. Once again using Legendre polynomials the real magnetic field can be approximated as [Kett 14]:

$$\vec{B}(\rho, \theta) = \vec{\nabla} \sum_{k=0}^{\infty} \frac{B_k}{k+1} r^{k+1} P_{k+1}(cos\theta) \ , \tag{2.14}$$

with B_k as the strengths of the different orders of the approximation series. B_0 describes the ideal homogeneous field, so the orders $k = 1$ and 2 are the dominant orders of inhomogeneity. In the case of a symmetric trap the B_1-term averages out due to the circular motion of the ions. However, dislocation of an ion's equilibrium position could result in frequency shifts due to a non vanishing B_1-term. This can be the case if switching between different ion species (see Sec. 3.4).

2.2.3 Voltage stability

The imperfect voltage stability, even though being constantly improved by more and more stable sources e.g. the ultra-stable voltage source StaReP [Böh 16], brings in small frequency shifts[1]. Since this work deals with environmental shifts including temperature changes, which can influence the electronic components, these shifts need to be taken a closer look at (adapted from [Dör 15]). The shifts can be calculated from Eq. (2.7) and Eq. (2.6):

$$\Delta\nu_z = \nu_z \frac{\Delta V_0}{2V_0} \ , \tag{2.15}$$

$$\Delta\nu_\pm = \mp \frac{\nu_z^2}{\nu_+ - \nu_-} \frac{\Delta V_0}{2V_0} \ . \tag{2.16}$$

If not simultaneously measured (the measurement schemes will be described in Sec. 3.4), the shifts of the eigenfrequencies do not equal out in the invariance theorem (Eq. (2.10)). Calculating ν_c, the largest shifts, due to the scale of the frequencies ($\nu_+ \gg \nu_z \gg \nu_-$), stem from the influence of the voltage instability on ν_+:

$$\frac{\Delta\nu_c}{\nu_c} = -\left(\frac{\nu_z}{\nu_c}\right)^2 \frac{\nu_+}{\nu_+ - \nu_-} \frac{\Delta V_0}{2V_0} \ , \tag{2.17}$$

and on ν_z:

$$\frac{\Delta\nu_c}{\nu_c} = \left(\frac{\nu_z}{\nu_c}\right)^2 \frac{\Delta V_0}{2V_0} \ . \tag{2.18}$$

Whereas only a small shift is due to the magnetron frequency:

$$\frac{\Delta\nu_c}{\nu_c} = \left(\frac{\nu_-}{\nu_c}\right)^2 \frac{\nu_+}{\nu_+ - \nu_-} \frac{\Delta V_0}{V_0} \ . \tag{2.19}$$

How large these shifts can be in order to still reach the desired relative mass precision (at PENTATRAP below 10^{-11}) is calculated by using the frequency factors in Eq. (2.17) and Eq. (2.18), and the relative voltage stability, achieved by an ultra-stable voltage source. To reduce the influence of this shift on the cyclotron frequency measurement, a possibility due to Eq. (2.2) is to increase q/m by using highly charged ions as well as measuring ν_+ and ν_z quasi simultaneously (for more information on this see Sec. 2.3.3). The more stable the voltage source, the smaller the q/m can be for a desired precision or vice versa. The shift coming from small short-time fluctuations ($t \ll t_{meas}$) on the modified cyclotron frequency ν_+

[1] In the following the angular frequency ω and the actual measurable frequency $\nu = \frac{\omega}{2\pi}$ of the ion will both be referred to as frequency.

is averaged out by the measurement itself. Fluctuations on a long time scale, in comparison to which the measurement of the three frequencies can be called simultaneous, are equalized by the invariance theorem. So the most unstable time frame of the frequencies due to voltage fluctuations is in between the two. This time frame has to be taken into account during the environmental measurements concerning voltage fluctuations (e.g. temperature measurements).

2.2.4 Magnetic field stability

The magnetic field stability enters the precision of the cyclotron frequency directly via Eq. (2.2). So to get a relative cyclotron frequency precision of below 10^{-11} the same relative stability of the magnetic field at the position of the ions is necessary. The result is a need of a very strong superconducting magnet (7T at PENTATRAP), at maximum possible shielding, and an environment with a stable magnetic field. To what extend this is achievable will be described in Sec. 3.2 and Sec. 4.1

2.3 Ion detection and manipulation

In order to determine a frequency to high precision it is necessary to have a single ion in the trap, so that the ion is not influenced by Coulomb interactions with other trapped ions. The next section will describe how this ion is cooled, the eigenfrequencies are manipulated, and the frequencies and phases are detected. A more detailed description of the detection systems at PENTATRAP can be found in [Dör 15] or [Risc 18].

2.3.1 Ion detection

An ion moving in a trap induces image currents in the trap electrodes with the same frequencies as the corresponding eigenfrequencies. These image currents can be detected as a voltage drop over a parallel impedance, which is realized by a superconducting RLC circuit connected to a trap electrode. At PENTATRAP this RLC circuit is set up as an axial detection system by connecting it to a correction electrode (see Fig. 2.3). A single ion, even a highly charged ion, creates only a small image current so the signal needs to be further amplified, using a cryogenic and a room temperature amplifier before Fourier transforming the signal by a spectrum analyzer to a frequency spectrum. The RLC circuit is built in a way that its resonance frequency lies in the rough range of a typical axial frequency. This allows to tune the axial frequency of the ion to the circuit's resonance frequency by adjusting the trap voltages (see Eq. (2.7)). The signal of the hot ion with it's large axial amplitude is visible as a peak on the circuit's resonance curve (see Fig. 2.4 (red line)). The resonance curve is solely created by the resonant enhancement of the electronic thermal noise of the cryogenic detection circuit. With the axial detection circuit connected to the electrode, the axial motion of the ion is damped due to the interaction with the detection circuit. This resistive cooling results in the thermalization of the ion with the detection circuit to the same cryogenic temperature. After "cooling in", the ion appears as a dip on the resonance curve

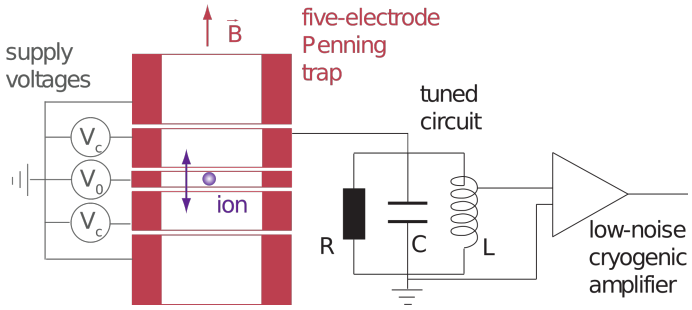

Figure 2.3: Schematic of an axial detection system used to detect single ion signals. The example shows the cylindrical trap geometry used at PENTATRAP with two correction electrodes and an RLC circuit connected to one of them. Behind the detection circuit a cryogenic amplifier with high ohmic input makes the voltages measurable. (Taken from [Repp 15])

as depicted in Fig. 2.4 (blue line). This non-destructive detection method is called Fourier-transform ion-cyclotron resonance or FT-ICR ([Wine 75] and [Jeff 93]).

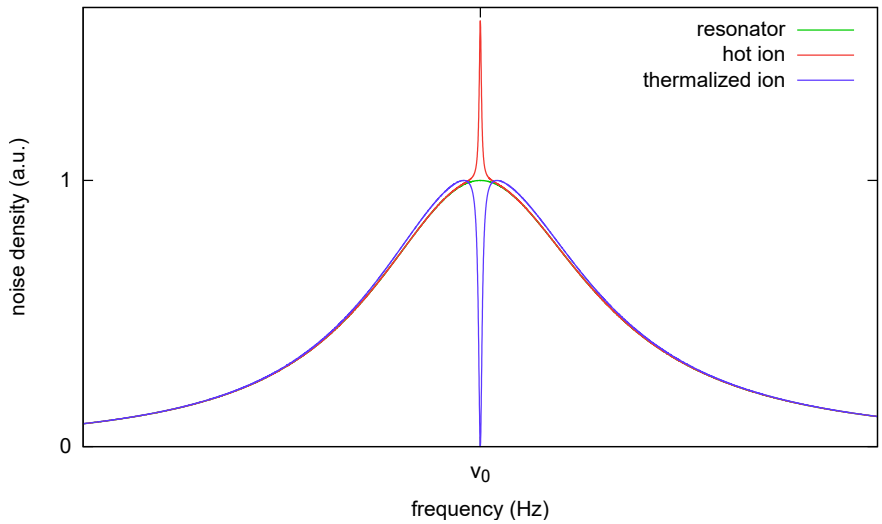

Figure 2.4: Calculated resonance curve of an axial detection circuit connected to a correction electrode (green line) superimposed with an eigenfrequency of the ion as a peak signal of the excited motion (red line) and as a dip signal of the cooled-in ion (blue line).

2.3.2 Excitation and Coupling

Dipolar excitation

If applying an RF (short for radio-frequency) field to an electrode with a frequency at/near one of the eigenfrequencies of the ion, it will excite the corresponding eigenmotion. For axial excitation the radio frequency is applied to an endcap or a correction electrode. The radial modes need a split electrode for

excitation. This dipolar excitation is useful for imprinting a certain phase on one of the ion's eigenmotions (necessary for PnP method see Sec. 2.3.3).

Quadrupolar coupling/excitation

If measuring the axial motion with an axial detection system, the other eigenmotions are manipulated or cooled by coupling them to the axial frequency with a quadrupole RF field. This coupling is achieved by applying an RF-field $\vec{E}_{ij}$ to a split correction or endcap electrode, corresponding to a quadrupolar excitation at the position of the ion:

$$\vec{E}_{ij}(t) = E_0 \cdot \sin\left(\frac{\nu_{\mathrm{rf}} t}{2\pi} + \phi_{\mathrm{rf}}\right)(x_i \vec{e}_j + x_j \vec{e}_i) \ , \tag{2.20}$$

with the coupling frequency ν_{rf} and its phase ϕ_{rf}. For coupling two eigenmotions the sum or difference frequency of the two eigenfrequencies is applied. For the duration of the coupling, the energy of the two modes is periodically transferred back and forth from one mode to the other, making it possible to transfer all the energy by coupling in a π-pulse. This concept can be used to cool down the radial modes by transferring their thermal energy to the resistively cooled axial mode.

For the determination of all three eigenfrequencies it is necessary to couple the radial modes to the axial mode: $\nu_{\mathrm{rf}} = \nu_{\pm} \mp \nu_z + \delta$ (δ is the offset to the resonant coupling). This will create Rabi oscillations, seen as a splitting of the single dip, with the frequencies of the left (ν_l) and right (ν_r) dip:

$$\nu_{l,r} = \nu_z - \frac{1}{2}\left(\delta \pm \sqrt{\Omega_0^2 + \delta^2}\right) \tag{2.21}$$

with the Rabi frequency $\Omega_0 = \frac{qE_0}{2m}\frac{2\pi}{\sqrt{\nu_z \nu_{\pm}}}$. If the coupling frequency is inserted in Eq. (2.21) one gets the following frequencies for the magnetron and modified cyclotron motion:

$$\nu_+ = \nu_l + \nu_r - \nu_z + \nu_{\mathrm{rf}} \ , \tag{2.22}$$

$$\nu_- = -\nu_l - \nu_r + \nu_z + \nu_{\mathrm{rf}} \ . \tag{2.23}$$

With this scheme it is possible to measure all three eigenfrequencies of the trapped ion with a detection system sensitive to just the axial motion.

2.3.3 Phase measurement

For a more precise measurement of the ion's free-space cyclotron frequency than with the dip method, the modified cyclotron frequency ν_+, which makes up its largest contribution, is measured with a phase method called Pulse and Phase (PnP) (specifics see [Corn 89]). It uses the fact that one can imprint a phase on an eigenmotion with a dipolar excitation and also transfer a phase from one eigenmotion to another. The method works as follows:

1. Imprinting a certain phase on the modified cyclotron motion by a dipolar excitation.

2. Letting the modified cyclotron phase evolve freely for a precisely known accumulation time.

3. Transferring the phase and energy of the modified cyclotron motion to the axial motion with a π-pulse.

4. Measuring the phase of the axial motion.

Since only the modulo of 2π of the total phase can be measured, the total phase ϕ_{total} following from this measured phase ϕ_{meas} is:

$$\phi_{total} = 2\pi N + \phi_{meas} \ , \tag{2.24}$$

with the integer N being determined by means of an additional measurement of the phase at different accumulation times, called *unwrapping measurement* [Risc 18]. With the total phase calculated and the precisely known accumulation time one can calculate the modified cyclotron frequency according to Eq. (2.6). For a reduction of the error due to axial frequency drifts the PnP measurement can even be combined with a quasi-simultaneous axial dip measurement during the accumulation time of the modified cyclotron phase (step 2).

Chapter 3

The mass spectrometer PENTATRAP

The Penning-trap mass spectrometer PENTATRAP aims at determining mass-ratios of long-lived highly-charged ions to a relative precision of below 10^{-11} by measuring the ratios of the ions' cyclotron frequencies. This challenging goal requires a combination of a room-temperature setup for the production, selection, and guidance of the highly-charged ions, as well as a cryogenic setup for the Penning traps and ion detection systems. This chapter gives an overview of the experimental setup of the room temperature and the cryogenic sections of the PENTATRAP experiment. The description of the experiment follows the ions' route from the ion source to the traps. A description of the measurement and mass-ratio analysis schemes will follow. The chapter closes with a description of the environmental sensors in the laboratory. A 3D model of the whole experiment is given in Fig. 3.1.

3.1 Ion production and transport

The start of the beamline of PENTATRAP is the ion production section, where electron beam ion traps (*EBITs*) are used to create clouds of highly-charged ions. An EBIT produces these highly-charged ions by electron impact ionization of a neutral atom cloud. In order to condense the electron beam and thereby increase the ionization cross section, a strong magnetic field is generated along the flight axis of the electrons. The ions are trapped with a superimposed electrostatic potential in axial direction and the negative space charge of the electron beam in radial direction (see Fig. 3.2). The trapping of the ions makes it possible to reach higher charge states because of sequential ionization. In order to extract the ions, the last drift tube towards the beamline is pulsed to a lower voltage than the central drift tube, thereby removing the potential barrier and accelerating the ions out of the trap and along the beamline. Of the two EBITs shown in Fig. 3.1, so far only the room-temperature Dresden EBIT (*DREEBIT*) is connected to the beamline. The Tip-EBIT is currently under commissioning and being connected to the

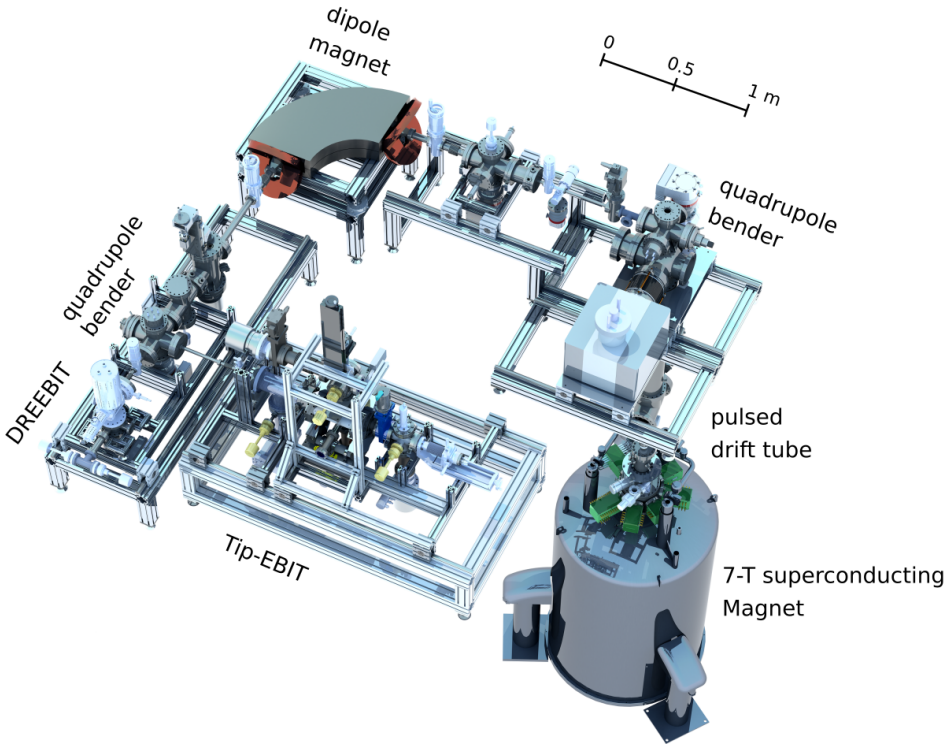

Figure 3.1: This 3D model shows the setup of the sections for ion production (DREEBIT and Tip-EBIT), ion species selection (dipol magnet) and guidance to the Penning traps inside the 7-T magnet on the floor below (quadrupole bender and pulsed drift tube). More information on the different sections can be found in the text.

PENTATRAP beamline [Schw 17, Kön 19]. This specially modified EBIT uses a laser ablation technique to ablate material off a needle tip, which is coated with a rare isotope, close to the trap center and then ionizes the ablated atoms. This technique minimizes the loss of atoms in the EBIT, making it possible to ionize materials even if they are only available in small sample sizes of $< 10^{12}$ atoms. As part of the ECHo collaboration which is aiming for the measurement of the electron-neutrino mass in the sub-eV range [Gast 17], the Tip-EBIT was developed to contribute the Q value of the artificially created ^{163}Ho [Dorr 18].

The beamline following the EBITs contains a combination of electrostatic einzel lenses and steerers to focus the beam onto the first diagnostics unit. A 90° dipol magnet for m/q separation enables the experimenter to choose the desired ion species by changing the applied current and thereby the magnetic field. The diagnostics unit allows to optimize the beam parameters in order to minimize the loss of ions and optimize ion species selection. Afterwards, when the desired beam is attained, the 90° vertical quadrupole bender guides the ion species of interest in the direction of the cryogenic setup (on the floor below). Before the Penning traps are reached, the ions have to be slowed down. With an energy of $q \cdot 6.5$ keV the ions enter two consecutive pulsed drift tubes, where they get decelerated to below $q \cdot 10$ eV, so they can be captured in the Penning traps. More diagnostic units between the pulsed drift tubes

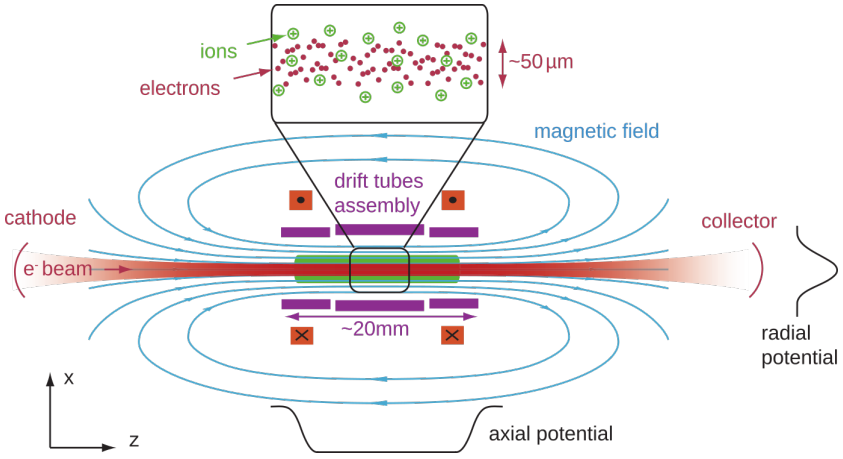

Figure 3.2: Schematic of an electron beam ion trap. The electron beam is created in the cathode, accelerated by the electrostatic potential difference of the cathode and the drift tubes, wherein the electron impact ionization of the neutral atoms takes place, before being extracted at the collector. After being ionized, the ions get drawn into the trap center by the negative space-charge of the electrons and the electrostatic potential applied to the drift tubes. (Taken from [Repp 15])

and below the traps allow to optimize the steering of the ion beam and timing of the pulsed drift tubes and to determine the ion flux along the z-axis and through the Penning traps.

3.2 The 7-T superconducting magnet

The magnetic trapping field of the Penning traps is created by a commercial 7-T superconducting magnet by *Varian* [Vari 15]. The magnet has a vertical bore with a diameter of 160 mm for the insertion of the Penning traps and the cryogenic detection systems. In order for the magnet's coils to be superconducting, they are submersed in liquid helium. The liquid helium is divided into two reservoirs, the magnet reservoir and the cold bore, which are connected at the bottom by a small capillary for liquid helium exchange. The dewar with the two reservoirs for the liquid helium will be described in more detail in Sec. 5.3.1. The magnetic field is highly homogeneous: $\Delta B/B$ is in the order of a few 10^{-6} in the central 1 cm^3 volume. Moreover, the magnet has a self-shielding capability through its own flux-stabilizing coil [Gabr 88]. The self-shielding is estimated by Varian to reach a shielding factor of >100 and thereby substantially reduces the influence of external magnetic field fluctuations on the trapped ions [Vari 15].

3.3 The Penning traps

PENTATRAP has, as the name already implies, a stack of five Penning traps available. They are cylindrical, compensated traps with five electrodes each. Stacked on top of each other, they can be used to measure the cyclotron frequency of several ions simultaneously, as well as moving the ions from trap to

trap to allow for elaborate measurement schemes for high-precision measurements of cyclotron-frequency ratios. Fig. 3.3 shows the trap tower and indicates some of the materials used in the setup. The traps as well as the cryogenic electronics connected to them (detection systems and amplifiers) are located in the cold bore of the magnet and submersed in liquid helium. The trap chamber is evacuated to an ultra-high vacuum by cryogenic pumping reaching a desired pressure of 10^{-15} hPa. For a complete description of the traps and their parameters see [Roux 12] and [Repp 15].

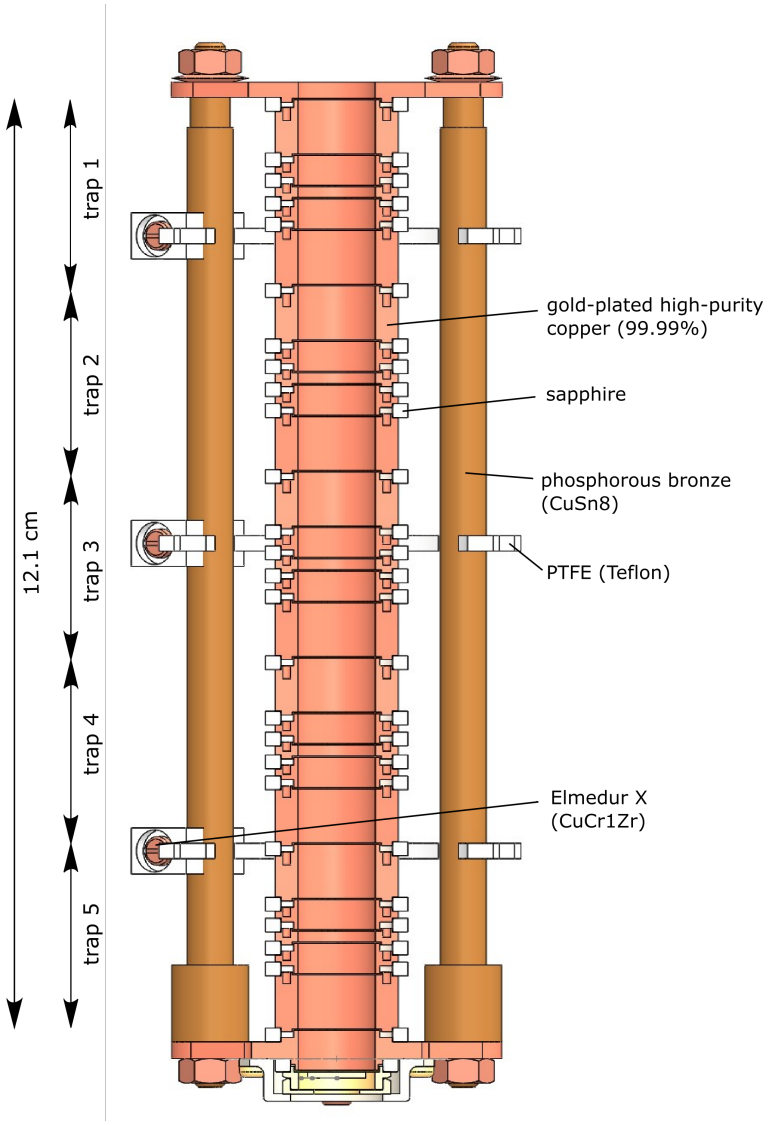

Figure 3.3: Drawing of a sectional view of the PENTATRAP trap tower. For details see [Repp 15].

Currently, traps 2 and 3 are used as cyclotron frequency measurement traps, while traps 1 and 4 serve as storage traps during the 2-trap measurement scheme, described in Sec. 3.4. Trap 5 is planned on being used as a monitor trap for fluctuations of the magnetic field or the trapping potentials supplied by the ultra-stable voltage source StaReP [Böh 15]. Tab. 3.1 lists the eigenfrequencies of a trapped $^{131}Xe^{17+}$-ion measured at PENTATRAP in the two measurement traps as an example of the scale of the

eigenfrequencies of ions in the Penning traps. They fulfill the frequency hierarchy in Eq. (2.11).

Table 3.1: Typical frequencies of a $^{131}Xe^{17+}$ ion in the two main frequency-measurement traps at PENTATRAP (trap 2 and 3). The eigenfrequencies were measured with a trap depth of $V_0 = -58.3$ V in trap 2 and $V_0 = -26.9$ V in trap 3.

	trap 2	trap 3
frequency	(Hz)	(Hz)
ν_-	$19.6 \cdot 10^3$	$9.1 \cdot 10^3$
ν_z	$740.0 \cdot 10^3$	$504.8 \cdot 10^3$
ν_+	$13.9453 \cdot 10^6$	$13.9558 \cdot 10^6$
ν_c	$13.9649 \cdot 10^6$	$13.9649 \cdot 10^6$

For traps 2 and 3 the magnetic field strength B_0 as well as the parameter quantifying the magnetic field inhomogeneity B_1 at the trap centers have been measured recently. Results are shown in Tab. 3.2. The table shows, that traps 2 and 3 have B_1 values with opposite signs. These values will be important in order to understand how some of the environmental parameters (e.g. pressure) influence the ion's eigenfrequencies (see Chap. 4).

Table 3.2: Magnetic field parameters of the two measurement traps. The values have been determined as part of the Master's thesis of M. Door [Door 18].

trap	B_0 (T)	B_1 (μT/mm)
2	7.002162294(5)	-1.539(84)
3	7.002168459(2)	1.446(72)

3.4 Measurement and analysis schemes at PENTATRAP

For the cyclotron frequency measurement, a 2-trap measurement scheme is currently used at PENTATRAP. Three single ions of two different ion species are loaded alternately into three of the five traps. In the first step, see position 1 in Fig. 3.4, the modified cyclotron frequency and axial frequency are measured in trap 2 and 3. Then, the ions are transported to position 2 and the frequencies are, once again, measured in trap 2 and 3 now with the ion species effectively switched (see Fig. 3.4). The ions are

then transported back to position 1 and the process is repeated. The modified cyclotron frequency and the axial frequency are measured by a PnP and simultaneous axial-dip measurement (see Sec. 2.3). In order to determine the cyclotron frequency of the ions, the magnetron frequency by means of a double-dip measurement and the phase-unwrapping measurement are carried out before every new measurement cycle. The phase-unwrapping measurement is necessary for the determination of the modified cyclotron frequency from the measured modified cyclotron phase. For a complete description of the measurement schemes and detection techniques at PENTATRAP see [Risc 18].
In order to reach a relative precision of below 10^{-11}, magnetic fields drifts need to be canceled out in the mass-ratio analysis. The above described measurement scheme allows to perform the analysis in two ways, indicated by the shaded squares in Fig. 3.4.

3.4.1 Polynomial method

For the polynomial method the cyclotron frequencies of position 1 and 2 for both traps are fitted with the same third-degree polynomial, but differing by an additional factor R for one of the two data sets. The order of the polynomial was chosen by a χ^2 test [Schu]. The ratio R then describes the cyclotron frequency ratio between the two positions and, since the ion species were changed between position 1 and 2, it also describes the frequency ratio of the two ion species. This analysis procedure interpolates the change in magnetic field by a polynomial.

3.4.2 Cancellation method

The analysis method that can potentially reach a higher precision, because it almost completely cancels out magnetic field drifts, is referred to as the cancellation method. It determines the cyclotron frequency ratios in traps 2 and 3, i.e. $R_1(t_1)$ and $R_2(t_2)$, of ion species A and B (see Fig. 3.4 for the definition of B fields and measurement times):

$$R_1(t_1) = \frac{\nu_{c,A}}{\nu_{c,B}} = \frac{m_B}{m_A} \cdot \frac{B_2(t_1)}{B_3(t_1)} \tag{3.1}$$

$$R_2(t_2) = \frac{\nu_{c,A}}{\nu_{c,B}} = \frac{m_B}{m_A} \cdot \frac{B_3(t_2)}{B_2(t_2)} \tag{3.2}$$

$$\Rightarrow \sqrt{R_1(t_1) \cdot R_2(t_2)} = \frac{m_B}{m_A} \cdot \sqrt{\frac{B_2(t_1)}{B_3(t_1)} \cdot \frac{B_3(t_2)}{B_2(t_2)}} \, . \tag{3.3}$$

With the ratio of the magnetic fields in trap 2 (B_2) and in trap 3 (B_3): $\frac{B_2}{B_3} \approx$ const. the magnetic field drops out:

$$\sqrt{R_1 \cdot R_2} = \frac{m_B}{m_A} \, . \tag{3.4}$$

The last step requires the same temporal behaviour of the magnetic field drifts in both measurement traps. This analysis scheme is potentially more precise, however, it is at the same time more vulnerable if the magnetic field drifts differently in traps 2 and 3, e.g. see Fig. 4.8.

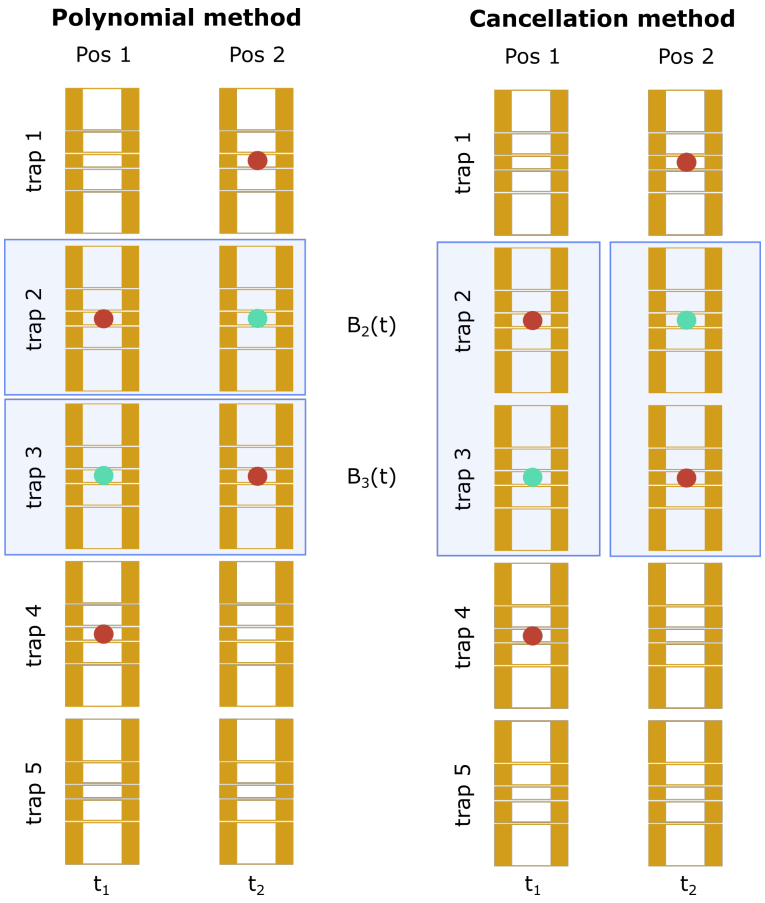

Figure 3.4: This figure shows a schematic representation of the 2-trap measurement scheme with two different analysis schemes which are currently used for mass-ratio determinations at PENTATRAP. The red and green circles mark ions of two different species A and B, respectively (different m/q). The shaded squares indicate which frequencies are analyzed together in order to obtain the mass ratio of the two ion species.

3.5 Environmental sensors

In the framework of this thesis, the PENTATRAP magnet laboratory has been equipped with temperature, pressure, and magnetic field sensors, as well as mass flow controllers for measuring/controlling the helium gas flow and a motion sensor. In the following, the sensors will be described. An overview of their position in the laboratory is given in Fig. 3.5.

3.5.1 Fluxgate magnetic field sensors

In order to measure the fluctuations of external fields in our lab, a magnetic field sensor is needed which picks up the slightest changes in the surrounding magnetic fields down to a few nanotesla magnetic field change. These fluctuations are measurable with certain fluxgate magnetometers which can achieve a resolution down to 20 pT with a measuring range of ± 100 μT [Stef]. The functioning principle of such a

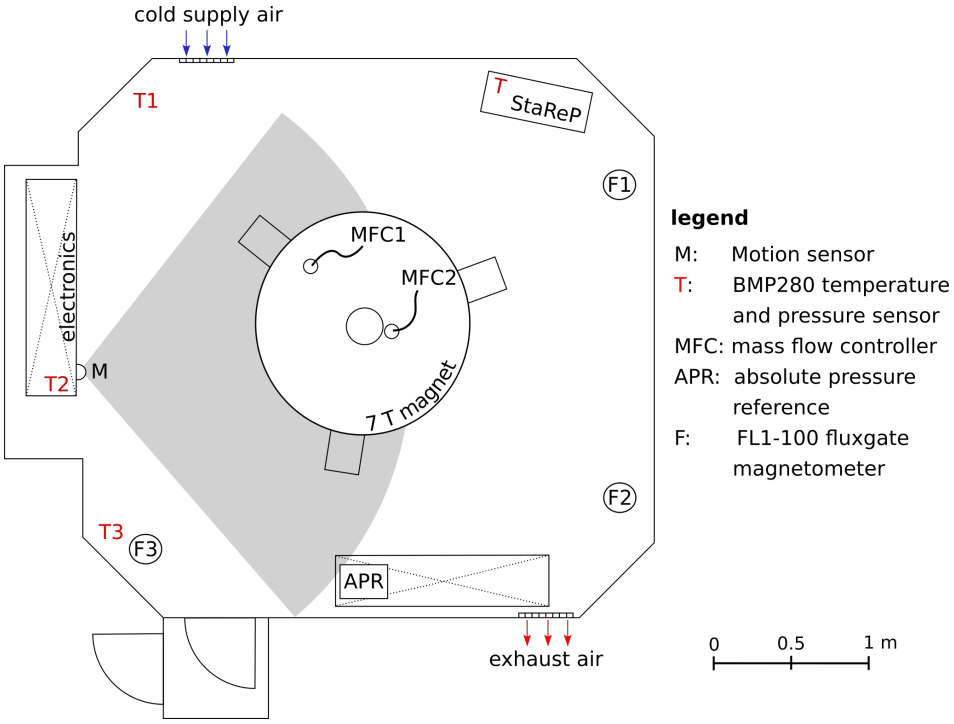

Figure 3.5: This sketch depicts a bird's eye view of the laboratory. The positions of the different environmental sensors, set up during this thesis, around the PENTATRAP magnet are marked. The absolute pressure reference is used for the pressure stabilization system (only partially included in the sketch). The sketch is approximately to scale.

sensor is the following: it consists, as visible in 3.6a, of an excitation and a sensing coil wrapped around two sides of a magnetically susceptible core. By applying an alternating current $I_{\text{exc}}(t)$ to the excitation coil, the core is periodically driven into saturation in both directions. According to Faraday's law, a changing magnetic field induces an electric force. In the case of no external field this electric force cancels out to zero between the two sides of the core, so no current is measurable in the sensing coil. In the case of an external field the two sides of the core reach saturation at different times, since on one side the external magnetic field is added to the excitation field while on the other it is subtracted from it. When reaching saturation at different times, the electric force between the two rods no longer cancels out, so the sensing coil will measure an electric potential. This measured voltage V_{sense} is proportional to the external magnetic field:

$$V_{\text{sense}}(t) = nA\mu_0 H_{\text{ext}} \frac{\mathrm{d}\mu_e}{\mathrm{d}t} \ , \tag{3.5}$$

with n the number of windings of the sensing coil, A the cross-sectional area of the core, μ_0 the permeability of free space, H_{ext} the external magnetic field to be measured, and μ_e the permeability of the core which depends on the current applied to the excitation coil.

FL1-100

For the measurement of external magnetic field changes in the laboratory, three fluxgate magnetometers of the type FL1-100 by *Stefan Mayer Instruments* [Stef] were installed around the experiment, as shown in Fig. 3.5. These low-noise fluxgate sensors with sub-nanotesla resolution can measure any relevant magnetic field fluctuation in the laboratory and can potentially be used for a magnetic field stabilization system due to their high resolution with fast measurement times.
To improve their temperature stability the sensors were installed as part of a sensor unit, including the actual sensor with its cabling (see Fig. 3.6b) and a cylindrical housing which is filled with sand as thermal mass. A pair of small Helmholtz coils are wrapped around the housing, which can be used to zero the magnetic field at the position of the sensors inside, in case the fluxgate needs to be used in an environment of a higher magnetic field, e.g. near the wall to the neighbouring experiment ALPHATRAP which uses a badly shielded 3.6 T magnet. These null coils can also be used as part of an active magnetic field stabilization, described in Sec. 5.1.

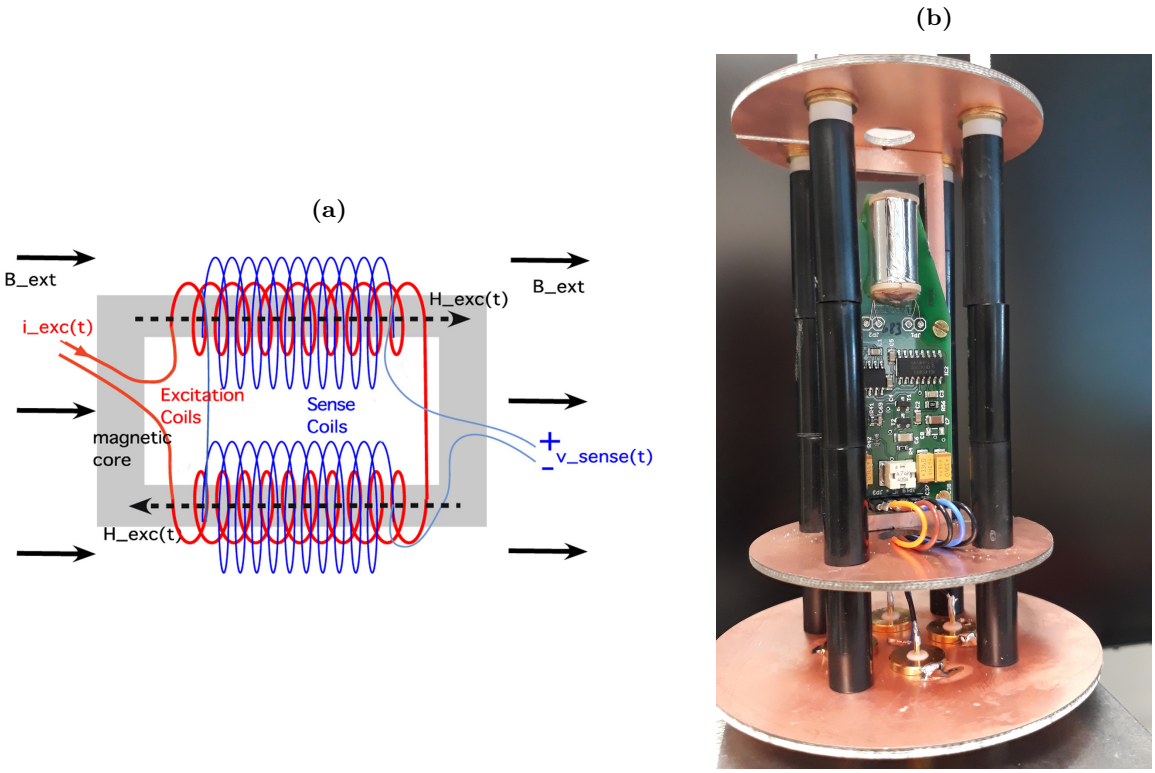

Figure 3.6: a) Working principle of a fluxgate sensor: An external magnetic field is measured by an excitation coil periodically driving a magnetically susceptible core into saturation and a sensing coil picking up an electric potential. More information can be found in the text. Figure taken from [Chit 17]. Photo b) shows the fluxgate sensor of type FL1-100 [Stef] as part of the sensor unit. The cylindrical housing and the null coils around it are not included in the picture

3.5.2 Pressure and temperature sensors

BMP280

The BMP280 [Bosc] is a compact absolute barometric pressure sensor which is installed in the laboratory at several different locations, in order to continuously log temperature and ambient pressure. The sensor has a relative accuracy of ±0.12 hPa at 950-1050 hPa and temperatures of 25-40 °C. Its pressure resolution is 0.01 hPa and the temperature resolution is 0.01 °C.

120AD and APR

For a more precise pressure measurement, e.g. for the purpose of a pressure stabilization, the differential pressure transducer 120AD by *MKS Instruments* [MKS a] is used in combination with an absolute pressure reference (*APR*). The 120AD sensor has a relative pressure resolution of $1 \cdot 10^{-6}$ over the full scale, which can be adjusted over five decades: smallest full scale of 1.33 hPa.

Chapter 4

Environmental influences

In this chapter, the systematic uncertainties of the cyclotron frequency determination stemming from environmental influences including the magnetic field, temperature and ambient pressure fluctuations are being examined in order to find possible correlations to fluctuations in the eigenfrequencies of the ions in the Penning traps. This will determine if further stabilization of the environmental influences or counter-measures will be necessary and to what extent.

4.1 Magnetic field fluctuations

Since the cyclotron frequency is proportional to the magnetic field (see Eq. (2.2)), it is imperative to have a highly stable field, resulting in the necessity to be aware of any magnetic field fluctuations or drifts. To reach the desired relative cyclotron frequency precision of below 10^{-11} with the PnP measurement scheme (described in Sec. 2.3.3), a limit should be determined for external magnetic field fluctuations. As described in Sec. 2.3.3 the total phase is calculated as $\phi_{total} = 2\pi N + \phi_{meas}$. If the shift of the measured phase, due to magnetic field drifts, becomes too large ($> 180°$), N will no longer be clearly determinable, resulting in an incorrect analysis of the total phase and thereby the modified cyclotron frequency. Taking a phase shift of 180° as the upper limit, Fig. 4.1 shows the maximum external magnetic field shifts for a range of different ion species (different m/q) at several phase accumulation times, calculated by:

$$\Delta B_{ext,max} = S \cdot \frac{m}{q} \frac{\Delta\phi_{max}}{t_{acc}} = S \cdot \frac{m}{q} \frac{\pi}{t_{acc}} \ , \tag{4.1}$$

with the shielding factor S of the superconducting magnet (description of self-shielding in Sec. 3.2).

If the fluctuations exceed these limits, an active stabilization of the external magnetic field or a reduced phase accumulation time will be necessary. In this chapter some of the most prominent causes of fluctuations seen in PENTATRAP's laboratory will be described.

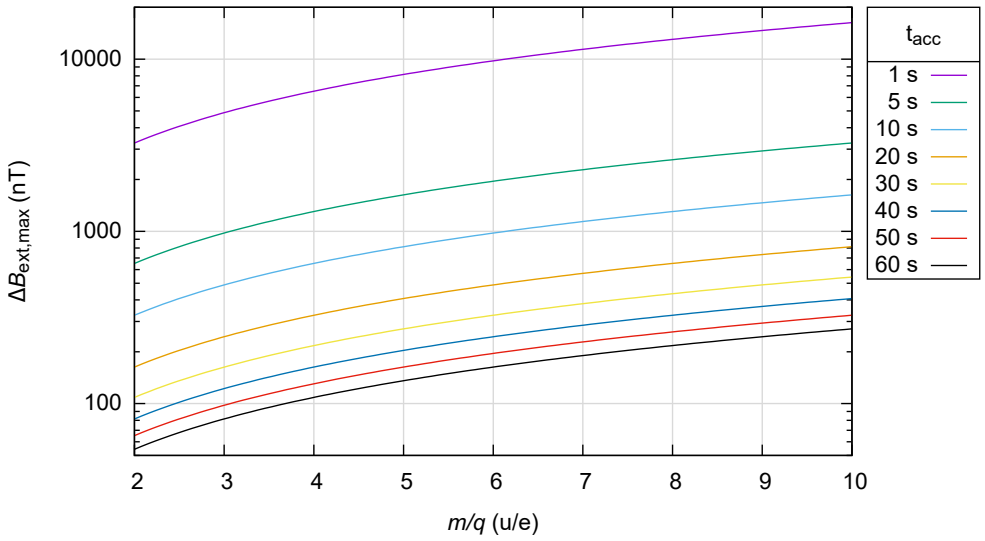

Figure 4.1: This figure shows the limits of external magnetic field shifts for a range of mass-to-charge ratios at different phase accumulation times t_{acc}. The limiting factor is the prevention of a π-shift in the modified cyclotron phase. The stability should be met over the time scale for one ν_c-determination cycle ($\sim$30 min) at best. The calculation was done with a shielding factor of $S = 50$.

4.1.1 Variation in the earth's magnetic field

In January 2018, the earth's magnetic field in z-direction at the location of the MPIK was, according to the world magnetic model calculator, $B_z = 44.05 \pm 0.16$ μT [NOAA]. The field amplitude is influenced by solar activity via energy transfer between solar winds and the earth's magnetosphere [Schm 85]. The resulting variations are visible in the laboratory by day-night fluctuations as seen in Fig. 4.2. The amplitude is changing slightly from day to day, depending on solar activity (larger amplitude on days with more solar flares and/or solar storms), as well as from winter to summer, due to the direction in which solar winds are hitting the magnetosphere. Typical amplitudes of these daytime magnetic field fluctuations lie between 10 and 40 nT during daylight on each day.

4.1.2 Identification of specific sources of magnetic field fluctuations

The MPIK being well-situated in the forest at the foot of the Königsstuhl, away from traffic and the city, has fewer environmental influences to be aware of than an institute directly in the city. However, there are still several location specific magnetic field disturbances that have to be accounted for.
During the night, when sources of larger field disturbances are not present, a substructure becomes visible, showing that fast field fluctuations between 2 and 4 a.m. are minimal (below 0.5 nT/min peak to peak). They increase to $\sim$ 2 nT/min peak to peak between 1 and 2 a.m. and 4 and 4:30 a.m. (see Fig. 4.3). Another increase up to 7 nT/min peak to peak takes place before 1 and after 4:30 a.m., correlating with

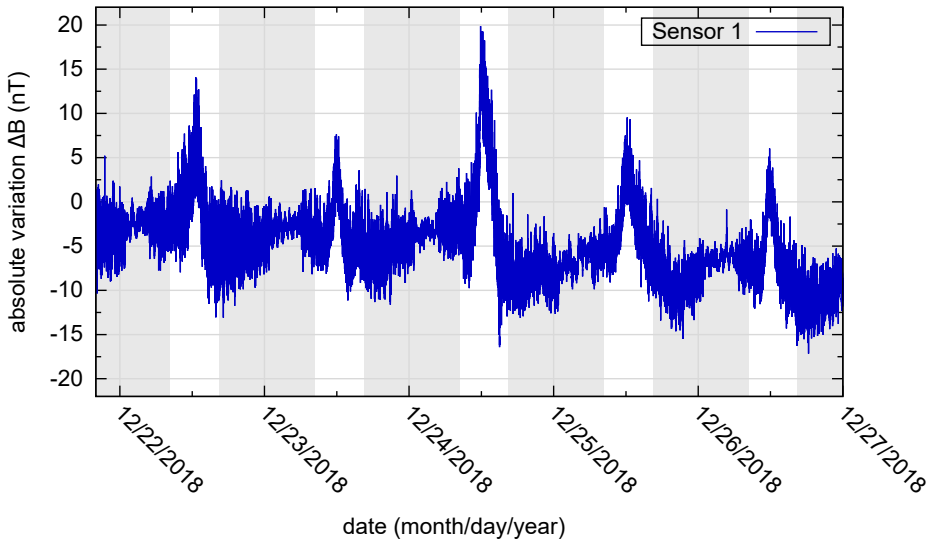

Figure 4.2: Absolute magnetic field fluctuations due to changes in the earth's magnetic field in the laboratory at the end of December 2018 are shown, when other influences on the magnetic field were at a minimum due to the holidays. The time between sunset and sunrise is shaded, showing the lower magnetic field changes during the night.

the schedule of the tram line 23 which passes by the institute at a distance of 1.4 km (shaded region in Fig. 4.3 indicates when the tram is running) [VRN].

In order to reassure the fluctuations do not stem from any common systematic errors, e.g. ground fluctuations, some additional test measurements were conducted. Decoupling the magnetic field sensor setup from the electric grid by using an uninterruptible power supply (UPS), as well as turning one magnetic field sensor upside down and comparing its output to the other two, proved the fluctuations were indeed magnetic field fluctuations. Positively identifying the source of these magnetic field fluctuations has proven difficult. However, considering the fact that the fluctuations match the time the tram is running, including the different schedules on Saturday/Sunday and public holidays (see example in Fig. A.1), the fluctuations most likely originate in the tram operation somehow. The scale of the fluctuations lie below the given limit on external magnetic field changes in Fig. 4.1 during high-precision frequency-ratio measurements, described in Sec. 4.1 and therefore do not limit the precision.

Close proximity to other experiments

As the PENTATRAP laboratory is located in the basement of the institute's experimental hall, it gets influenced by fringe fields of several other nearby experiments using strong magnets. For example the Heidelberg-EBIT with its up to 9 T strong superconducting magnet is powered up or down every week [Cres 04] and is located in close proximity to the Penning traps (a few meters above), creating field shifts in our laboratory of up to 7 μT over half an hour. Another source which creates field fluctuations is the

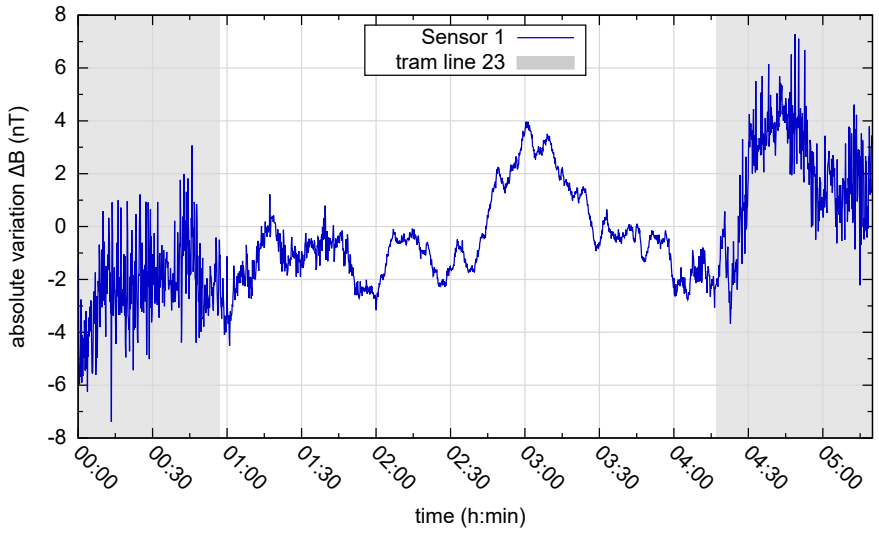

Figure 4.3: The external magnetic field variation in the laboratory during the night of April 10, 2019 is shown. Amplitude changes are visible in the fast fluctuations. The shaded regions indicate when the tram line is running.

ferromagnetic heavy-duty crane, bending the surrounding magnetic field lines when moving along the ceiling of the building. Furthermore, there are disrupting fields or field fluctuations in the lab during working days, created by work being done around the experimental hall above or in the adjacent labs of the Penning-trap experiment ALPHATRAP. In Fig. 4.4 a few field changes from identified sources are shown as well as an exemplary magnetic field measurement during a typical working day. The plotted magnetic field fluctuations exceed the limit on external magnetic field fluctuations (or get close to the limit), set for high-precision frequency-ratio measurements at PENTATRAP, described in Sec. 4.1. It is therefore advisable to measure during the night or on the weekends, while measuring without an active compensation, and to continuously monitor the magnetic field to be able to exclude data taken during large magnetic field jumps.

4.1.3 Shielding factor determination

External magnetic field drifts induce a cyclotron frequency shift on the trapped ions. According to Eq. (2.2), the cyclotron frequency scales linear with the magnetic field. However, as described in Sec. 3.2 the superconducting magnet shields the traps from external magnetic fluctuations by a shielding factor S. The shielding factor of PENTATRAP's superconducting magnet is position-sensitive and is therefore varying from trap to trap.

The calculation of the shielding factor can be done by analyzing phase measurements during large external magnetic field changes. Such a large magnetic field change is created when the Heidelberg EBIT's magnet is energized or deenergized (exemplary ramp down is shown in Fig. 4.4a). The external magnetic field change, due to the EBIT's decreasing fringe field, was interpolated to be $\Delta B_{ext} = (0.137 \pm 0.013)\ \mu$T/min

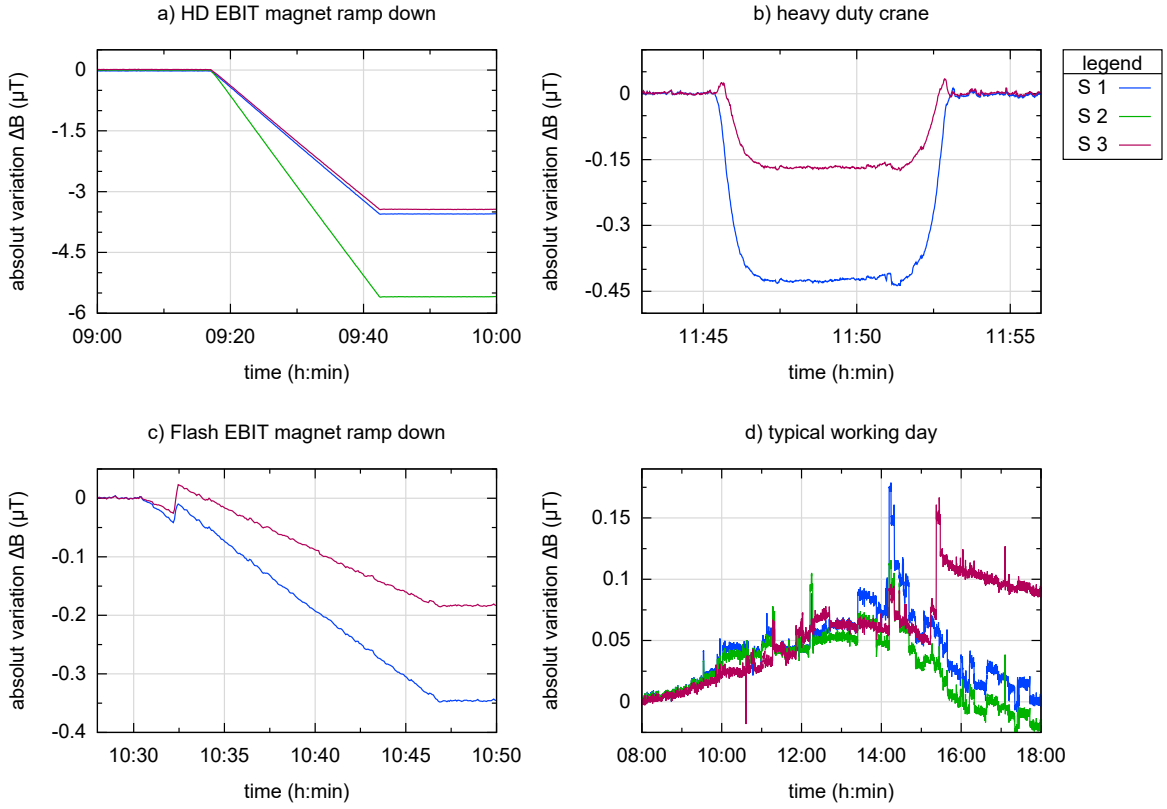

Figure 4.4: This plot shows different external magnetic field changes measured by the fluxgate sensors around PENTATRAP, caused by the surroundings of the laboratory (note different scalings). The magnetic field fluctuations come from a) the Heidelberg EBIT's 9 T magnet being ramped down, b) the heavy duty crane being moved over the lab, c) the Flash EBIT's magnet being ramped down and d) other unidentified sources during a typical working day.

at trap position. Used for the interpolation were the three fluxgate magnetometers in the PENTATRAP laboratory, which are all installed in the horizontal plane of the central trap (for location see Fig. 3.5). During the external magnetic field shift, a correlated phase shift in the modified cyclotron phase $\Delta\phi(\nu_+)$ was measured. The phase shift corresponds to a shift in the ion's magnetic trapping field of:

$$\Delta B_{ion} = 2\pi \frac{m}{q} \Delta\nu_c = \frac{m}{q} \frac{\Delta\phi}{t_{acc}} \left(2 - \frac{\nu_c}{\nu_+}\right) , \tag{4.2}$$

with t_{acc} being the phase accumulation time used during the measurement. This magnetic field shift calculation assumes that $\Delta\nu_z = 0$ and $\Delta\nu_- \ll \Delta\nu_+$, which applies for all traps at PENTATRAP. With the factor $(2 - \frac{\nu_c}{\nu_+}) \approx 1$ (in trap 2: 0.999 and in trap 3: 0.9995 for $\frac{m}{q} = \frac{187u}{29e}$ corresponding to $^{187}\mathrm{Re}^{29+}$) the magnetic field shift is:

$$\Delta B_{ion} \approx \frac{m}{q} \frac{\Delta\phi}{t_{acc}} . \tag{4.3}$$

With a measurement of a $^{187}Re^{29+}$ ion in one trap and a $^{187}Os^{29+}$ ion in the other trap, coinciding with a Heidelberg EBIT magnet ramp down, the shielding factors were determined, with $S = \frac{\Delta B_{ext}}{\Delta B_{ion}}$ to be:

$$\text{trap 2: } S = 55.9 \pm 3.4$$
$$\text{trap 3: } S = 50.3 \pm 3.0 \text{ ,}$$

with the largest contribution to the error coming from the determination of ΔB_{ext}.

4.2 Temperature fluctuations

External temperature changes are caused, among others, by the weather, temperature of the surrounding labs and hallways, the heat load of electrical components in the lab, as well as the lab door opening, causing an air stream of different temperature. Continuous temperature measurements at different locations in the laboratory showed a correlation of temperature to the measured eigenfrequencies, leading to several tests in order to improve the temperature stability. For more information on this temperature stabilization see Sec. 5.2.
While external magnetic field fluctuations directly influence the trapped ions, temperature fluctuations can indirectly influence the electric as well as the magnetic trapping fields. In the following some of the most likely scenarios of how the external temperature can influence the ions' eigenfrequencies in the Penning traps are described.

4.2.1 Temperature-induced voltage fluctuations

The ultra-stable voltage source StaReP [Böh 16], supplying the DC trapping voltages, was measured in the past to have a relative temperature dependence of $3.3 \cdot 10^{-6}$/K. The main contributor to this was the reference module with $2.7 \cdot 10^{-6}$/K, while the influence of the channels was only $0.3 \cdot 10^{-6}$/K. In December 2018, the former reference module based on VRE102 voltage reference integrated circuits (ICs) [Apex] was replaced by a new, more stable one, based on the LTZ1000 voltage reference ICs [Line]. The temperature dependence of StaReP's output voltages can be seen in all three eigenfrequencies, including the axial frequency following Eq. (2.7).

Temperature dependence measurements

Part of this thesis was dedicated to determine the temperature dependence of StaReP directly with a simultaneous temperature and axial-frequency measurement. This was done by changing the set point of the temperature stabilization in the lab by several degrees, causing a temperature curve and simultaneously measuring the axial frequency of a $^{187}Re^{29+}$ ion in each of the measurement traps. The result of one

of the temperature curves can be seen in Fig. 4.5. With Eq. (2.15), the relative temperature dependence of the DC trapping voltage was calculated to be:

$$\text{trap 2: } \frac{\Delta V_0}{V_0} = 2 \cdot \frac{\Delta \nu_z}{\nu_z} = (1.38 \pm 0.14) \cdot 10^{-6}/\text{K} \tag{4.4}$$

$$\text{trap 3: } \frac{\Delta V_0}{V_0} = (2.43 \pm 0.14) \cdot 10^{-6}/\text{K} \, . \tag{4.5}$$

The difference between trap 2 and 3 is due to the different channels used for each trap. The 25 channels in total (5 for each trap) have a maximum stability at a certain temperature. However, these optimum temperatures vary from channel to channel, resulting in a different temperature dependence in each trap. A characterization of the different channels can be found in the PhD thesis of Ch. Böhm [Böh 15]. Part of these temperature dependence measurements was also measuring the output of the reference or

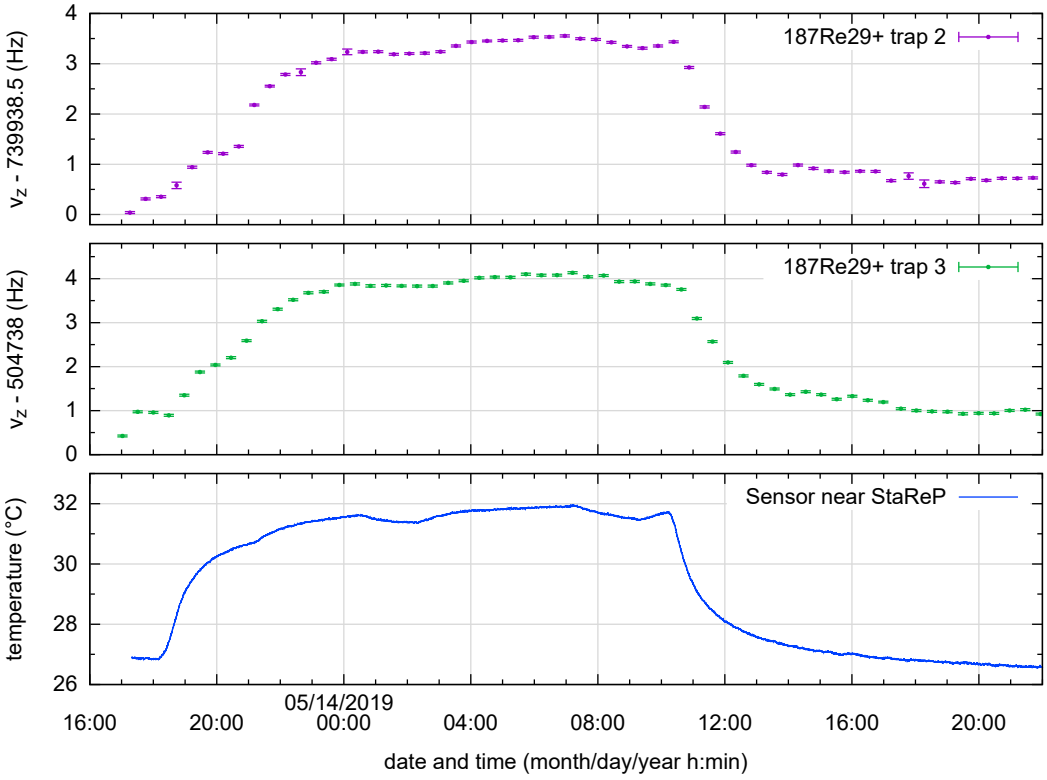

Figure 4.5: Temperature dependence measurements using the air conditioning to induce a temperature curve, while measuring the axial frequency ν_z of a $^{187}Re^{29+}$ ion in alternating traps.

one of the channels of StaReP with the reference multimeter FLUKE 8508A [Fluk], to test which of the components contributes most to the temperature dependence of the trapping voltages. The new temperature stabilized reference module had a much improved relative temperature dependence of below

$0.01 \cdot 10^{-6}$/K (see Fig. A.2) in comparison to the old reference module, whereas the channel under investigation contributed $< 20 \cdot 10^{-6}$/K to the overall temperature dependence (see Fig. A.2).

Necessary temperature stability

When aiming for a high-precision mass-ratio measurement, the cyclotron frequency-ratio needs to be measured to a high precision, i.e. below 10^{-11}. When looking at the temperature dependence of the ion's eigenfrequencies due to the trapping voltages fluctuating with temperature, all three eigenfrequencies contribute to the relative cyclotron frequency shift, see Eqs. (2.17), (2.18) and (2.19). The magnetron frequency's contribution is only relevant for large temperature changes. For simultaneous measurements of all three frequencies the shifts cancel each other out, due to the invariance theorem (Eq. (2.10)), leaving the cyclotron frequency unchanged. In the PnP-measurement scheme employed at PENTATRAP, the axial and modified cyclotron frequencies, contributing the largest shifts, are therefore measured quasi-simultaneously: the axial frequency is being measured during the phase accumulation time of the modified cyclotron phase (PnP-measurement scheme explained in Sec. 2.3.3). In order to quantify the impact temperature changes still have on the PnP-measurement scheme, three main precision-limiting factors can be accounted for.

The first limiting factor: If there is a temperature change within the short time between the end of the axial frequency measurement and the modified phase readout (currently set to $0.1 \cdot t_{acc}$), it would not cancel out in the invariance theorem. This means a high temperature stability is needed, only allowing a small temperature shift on short time scales. These shifts in the modified cyclotron frequency will scatter as long as there are no periodic fluctuations in temperature. As can be seen in Fig. 5.8, there are no periodic fluctuations. Thereby these phase shifts should behave statistically and the uncertainty of the cyclotron frequency should reduce with the number of phase measurements.

The second limiting factor: As described before in Sec. 4.1, a phase shift of 180° in the modified cyclotron phase circumvents a correct analysis of the modified cyclotron frequency. For a correct analysis it is therefore necessary to prevent large jumps in temperature over the time of one cyclotron frequency determination cycle (∼30 min).

The third limiting factor: the magnetron frequency is currently only determined at the beginning of every new measurement cycle (approximately every 12 h). Since the influence of the magnetron frequency's shifts on the cyclotron frequency is small in comparison to the other two eigenfrequencies', this still allows large temperature jumps without limiting the overall precision.

As an example, the limits on temperature fluctuations for the three different time scales for a $^{131}Xe^{17+}$ ion as a result of the temperature stability of the trapping voltage are listed in Tab. 4.1. The maximum temperature shift for a sub 10^{-11} relative frequency precision is being referred to as ΔT_{max}.

These results showed a much-needed improvement of the temperature stability and led to several tests aimed at reducing temperature fluctuations in the lab and lowering the temperature dependence of StaReP. This will be described in detail in Sec. 5.2.

Table 4.1: The table lists the maximum-allowed temperature shifts for a $^{131}Xe^{17+}$ ion, calculated with the temperature dependence of the trapping voltages (StaReP) from Eq. (4.5) in trap 2, in order to remain below a relative frequency precision of 10^{-11}. Line 1 is calculated on the basis that the phase is averaged over N single phase measurements and with a phase accumulation time of 40.05 s. More information, including a description of the limiting factors, can be found in the text.

time scale		ΔT_{max} (°C)	limiting factor
< 4 s	time between ν_z and ϕ_+ measurement	$0.007 \cdot \sqrt{N}$	1: shifts in ν_+
< 30 min	ν_c determination cycle	0.466	2: shifts in ϕ_+ larger than π
> 12 h	time between ν_- measurements	1.4	3: ν_- seldom measured

4.2.2 Temperature-induced magnetic field fluctuations

Another way the external temperature could influence the PENTATRAP experiment is by changing the temperature in the magnet's cold bore. Since the materials used for the traps and the trap chamber have a temperature dependent magnetic susceptibility, a change in temperature inside the magnet will change the magnetic field in the trap.
Moreover, the trap is suspended off 1168 cm stainless steel and copper, which expands or contracts with temperature (the rest of the vertical beamline is mechanically decoupled by a bellow). This would change the position of the trap and, due to the slightly inhomogeneous magnetic field, would alter the magnetic field strength experienced by the trapped ion. Opposite signs of the cyclotron frequency shifts for traps 2 and 3 are expected, since the B_1 factors for those two traps have recently been shown to have opposite signs, see Tab. 3.2. However, this was not visible in any temperature measurements, including the one shown in Fig. 4.5.

4.3 Pressure fluctuations

The liquid helium reservoir and the magnet's cold bore are influenced by ambient pressure due to their connection to the outside via two pressure-relief valves opening at a pressure difference of about 10 hPa. Since the liquid helium is constantly boiling off, the valve is constantly open and the pressure inside the helium dewar is fluctuating with the ambient pressure. Due to atmospheric pressure, which changes with the weather, the ambient pressure can vary between 960 hPa to 1010 hPa with typical daily variations of around 5-10 hPa.

4.3.1 Pressure correlation measurements

To examine the pressure dependence of the ions' eigenmotions, several phase measurements of different isotopes of Xe ions were compared with the corresponding ambient pressure. Correlated trends of the cyclotron frequency in both traps were visible, consistent with the trends in the external pressure. In Fig. 4.6 the longest cyclotron frequency measurement of a $^{131}Xe^{29+}$ ion in trap 2 is plotted against the pressure measured by several sensors spread out over the laboratory (for location of the sensors in the laboratory see Fig. 3.5).

A possible correlation between the changing ambient pressure and the cyclotron frequency would be caused if the pressure was changing the temperature of the liquid helium and the liquid helium level. Thereby the temperature of the stainless steel suspension of the traps submerged in liquid helium and the trap chamber would change. The stainless steel and copper would expand or contract with temperature, mechanically moving the traps along the slightly inhomogeneous magnetic field. As described before in Sec. 4.2.2, this reasoning was again deemed unlikely since the frequencies in both traps behaved coherently during pressure fluctuations (see Fig. A.3) and the B_1 terms have opposite signs for traps 2 and 3 as seen in Tab. 3.2.

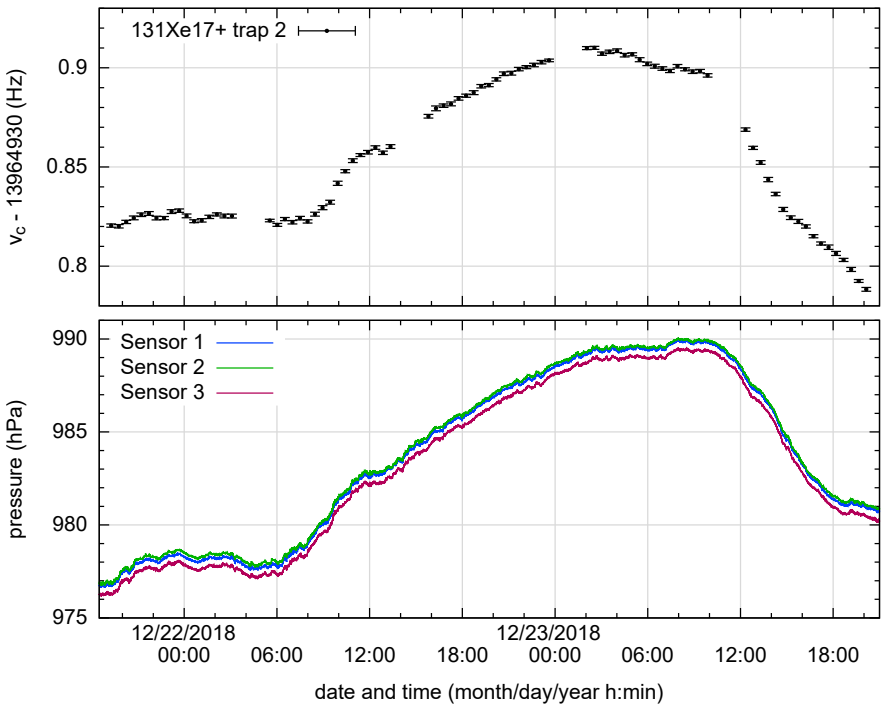

Figure 4.6: Ambient pressure fluctuations causing the cyclotron frequency of a $^{131}Xe^{17+}$ ion in trap 2 to drift over 1.5 days. The phase-unwrap measurement for trap 3 failed, therefore the cyclotron frequency could only be calculated for trap 2. The upper part shows the drifts in cyclotron frequency measured with a PnP measurement. The lower plot shows the external pressure fluctuations over the same time period, measured with three sensors of type BMP280 [Bosc].

Since both traps showed the same trends with similar amplitudes (see Fig. A.3), it was concluded that the pressure fluctuations cause the magnetic field in the cold bore to vary. The temperature in the cold bore is set by two factors: the evaporation temperature of liquid helium T_{evap}, which changes with pressure (at approx. $p = 1000$ hPa)

$$\frac{\Delta T_{evap}}{\Delta p} \approx 1 \frac{\text{mK}}{\text{hPa}} \tag{4.6}$$

and the helium level in the magnet's cold bore. Since some of the trap materials (see Fig. 3.3), e.g. high-purity copper 99.99%, have a temperature dependent magnetic susceptibility [Simo 92, Hurd 66], the magnetic field inside the traps fluctuates with the temperature. For a description of PENTATRAP's trap materials and their magnetic susceptibility see [Repp 15]. With the fluctuating magnetic field the connection is drawn between the ambient pressure and the cyclotron frequency (see in Fig. 4.6). To varify this conclusion and possibly get rid of the pressure induced frequency drifts, a helium-level and pressure stabilization system was connected to the cold bore and helium reservoir of the experiment. The description and results of this stabilization system will be described in Sec. 5.3.

4.4 Flow of evaporated helium

The flow of evaporated helium was measured using a flow controller which was installed in the exhaust system of the liquid helium dewar. The measurement of the flow of helium was conducted to see if there were any pressure build-ups in the dewar before the outlet valves opened, thereby influencing the experiment as described in Sec. 4.3.1. A somewhat similar behaviour of liquid helium flow and ambient pressure was visible (see Fig. 4.7). The flow was continuous, so the outlet valves are open constantly (to some degree) and the differential pressure between dewar (internal) and ambient pressure is constant. This establishes the connection of the phases to the ambient pressure (see Sec. 4.3). When reading out the helium level of the reservoir, the temporary increase of heat load causes a spike in the gas flow like the one seen in Fig. 4.7 on December 28. To avoid a permanently increased helium consumption, the helium-level stabilization system uses a capacitive level sensor (see Sec. 5.3). Moreover, the comparison between the two gas exhausts, one connected to the helium reservoir and the second to the cold bore, was of interest. As expected due to the thermal connection to the outside via the suspension and support of the trap in combination with the heat load of the cryogenic amplifiers and cabling (currently two amplifiers for two traps), the gas flow of helium out of the cold bore was much higher. No oscillations of gas flow magnitude between the two exhausts could be discovered. The average gas flow out of both outlets combined of 3500 ml/min corresponds to an approximate liquid-helium consumption of 7.2 l/day.

4.4.1 Helium level

The cancellation measurement scheme, described in Sec. 3.4, requires the same temporal behaviour in both measurement traps. If this requirement is met, the ratio evaluation allows the cancellation of the "global"

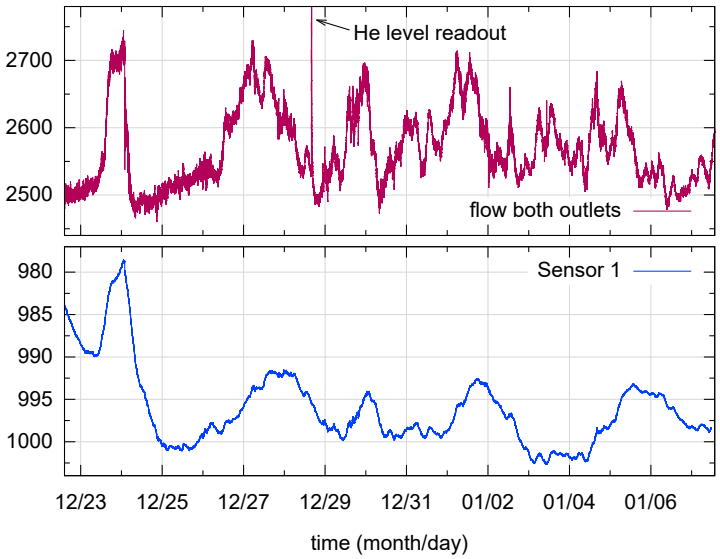

Figure 4.7: Comparison between flow of gaseous helium out of the cold bore and ambient pressure: Higher ambient pressure causes less gaseous helium to flow and vice versa.

magnetic field drift [Repp 12]. As soon as the cyclotron frequency in traps 2 and 3 no longer behaves coherently, this new measurement scheme cannot be used, meaning the loss of one of the advantages of having several measurement traps. As can be seen in Fig. 4.8, when the level of helium in the cold bore drops too low, the phases behave completely incoherently. This can be avoided by stabilizing the helium level, which was successfully tested. The stabilization system is described in Sec. 5.3.

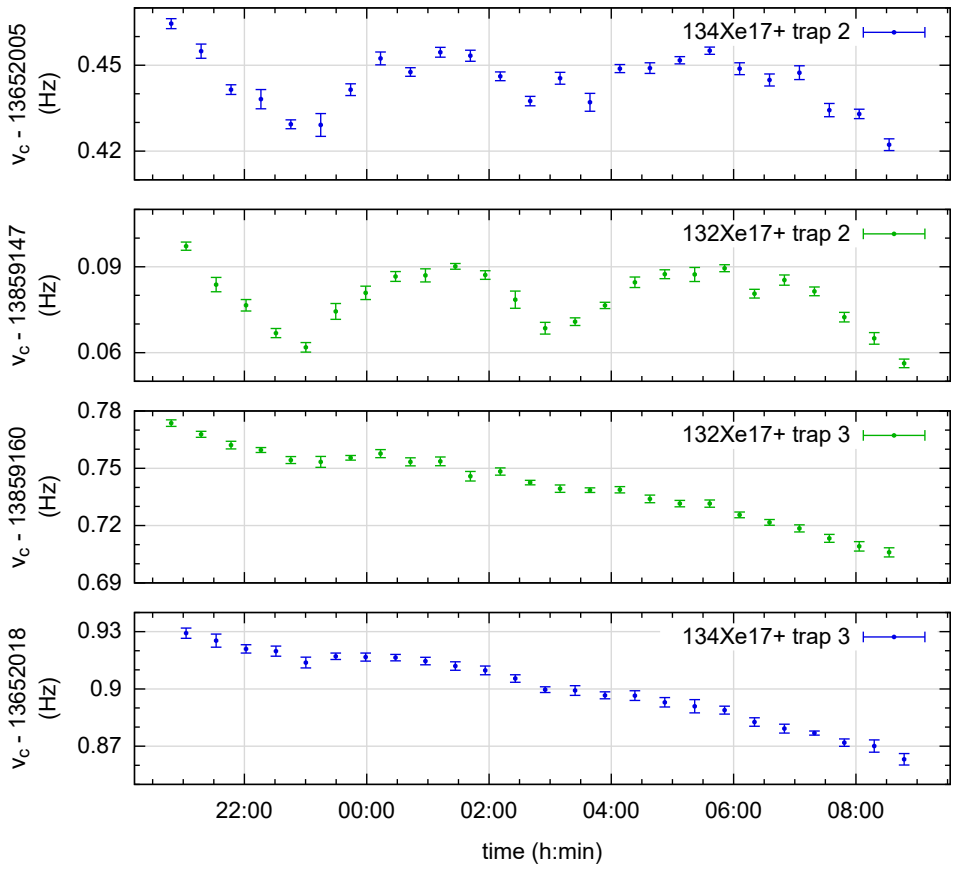

Figure 4.8: Cyclotron frequency measurement of a $^{132}Xe^{17+}$ and a $^{134}Xe^{17+}$ ion with a low helium level (shortly before a necessary helium refill). The cyclotron frequencies behave differently in traps two and three.

Chapter 5

Stabilization systems for environmental parameters

On the basis of the findings presented in Chap. 4, the following chapter will deal with the stabilization systems put in place and tested in the framework of this thesis. First, an active magnetic field stabilization system with Helmholtz coils will be described, then the temperature stabilization system in the laboratory and the changes made to it, as well as a cold bore helium-level and pressure stabilization system. In the end, the current status of the stabilization systems will be presented using a cyclotron frequency measurement in comparison to the measurement of the environmental parameters like temperature, pressure and magnetic field.

5.1 Active stabilization of the magnetic field

External magnetic field changes influence the magnetic trapping field by:

$$\Delta B_{trap} = \frac{\Delta B_{ext}}{S} \ , \tag{5.1}$$

with the shielding factor S of the superconducting magnet determined in Sec. 4.1.3. When the external fluctuations rise above the given limits on magnetic field fluctuations for high-precision frequency measurements, as shown in Fig. 4.1, an additional stabilization becomes necessary. One method of improving the magnetic field stability is to use an active stabilization system. The active stabilization system at PENTATRAP uses large Helmholtz coils, first built during the bachelor's thesis work of A. Rischka, centered around the magnet to counteract external magnetic field fluctuations [Risc 11].

Magnetic field fluctuations at the trap center can be monitored via the cyclotron frequency of an ion in the trap, e.g. in the monitor trap of PENTATRAP. In order to stabilize the magnetic field, however, a fast measurement of the magnetic field is needed, therefore excluding a double-dip measurement as an option. While a PnP measurement would qualify due to its adjustable phase accumulation time, the phase measurement's high sensitivity to the magnetic field would result in a failure of the stabilization if

the magnetic field shifts get too large, since shifts in the phase of larger or equal to 180° are no longer clearly identifiable. A PnP measurement on a monitor ion, e.g. in trap 5, would be suitable for measuring small magnetic field variations or slow magnetic field drifts. Very fast fluctuations cannot be resolved due to phase accumulation time necessary for a precise phase measurement. This might be helpful for the analysis of the cyclotron frequencies in the measurement traps. However, since the PnP measurement poses an upper limit on the scale of magnetic field shifts that can be measured, ions disqualify as a magnetic field sensor for the active stabilization system. Therefore, the magnetic field cannot be measured at the center of the Helmholtz coils, i.e. trap position, but instead has to be measured from the outside and only *global* magnetic field changes can be compensated. A magnetic field change is called global, when it is identical in z-direction in the midplane of the Helmholtz coils over the distance between the outside sensor used for the stabilization and the trap position. In the following, a test setup will be described which has been used to analyze how the external magnetic field measurements can be used for a compensation of the magnetic field fluctuations at the center of the Helmholtz coils.

5.1.1 Test setup with PID-controlled magnetic field compensation coils

The active stabilization system is made up of three main parts, as visible in Fig. 5.1:

- The magnetic field test setup, consisting of three FL1-100 fluxgate sensors [Stef], their respective null coils (description in Sec. 3.5.1), the large Helmholtz coils with a diameter 1.8 m and $N \sim$600 turns each, and an additional fluxgate sensor at the center to replace the ion in the trap.
- The electronic components necessary for the stabilization system: multimeters of the type 34470A by *Keysight* [Keysb] for the readout of the fluxgate sensors, a frequency generator of the type 33522B by *Keysight* [Keysa] as a digital to analog output converter, and the voltage-controlled precision current supply TOE 8733 by *Toellner* [Toel] for the null coils and the Helmholtz coils.
- The proportional–integral–derivative controller (*PID*) running on a remote computer. From the magnetic field sensor inputs, the PID is calculating the varying currents to compensate the magnetic field at the center of the Helmholtz coils and at the center of the null coils.

Since a magnetic field sensor at the center of the Helmholtz coils was needed during the test measurements in order to replace the trapped ion, the setup was moved just outside the laboratory ($\sim$5 m). This ensured similar magnetic field fluctuations as in the laboratory, while having space at the center of the Helmholtz coils to install a magnetic field sensor.
The goal of the test setup was to find a way to reliably stabilize the magnetic field at the trap position without having neither a magnetometer at that position nor an ion as a sensor. This external stabilization system has two main requirements: Firstly, a constant scaling factor between the current needed for zeroing of the outside sensor I_{null} and the current sent through the Helmholtz coils I_H:

$$I_H(t) = C \cdot I_{null}(t) \ . \tag{5.2}$$

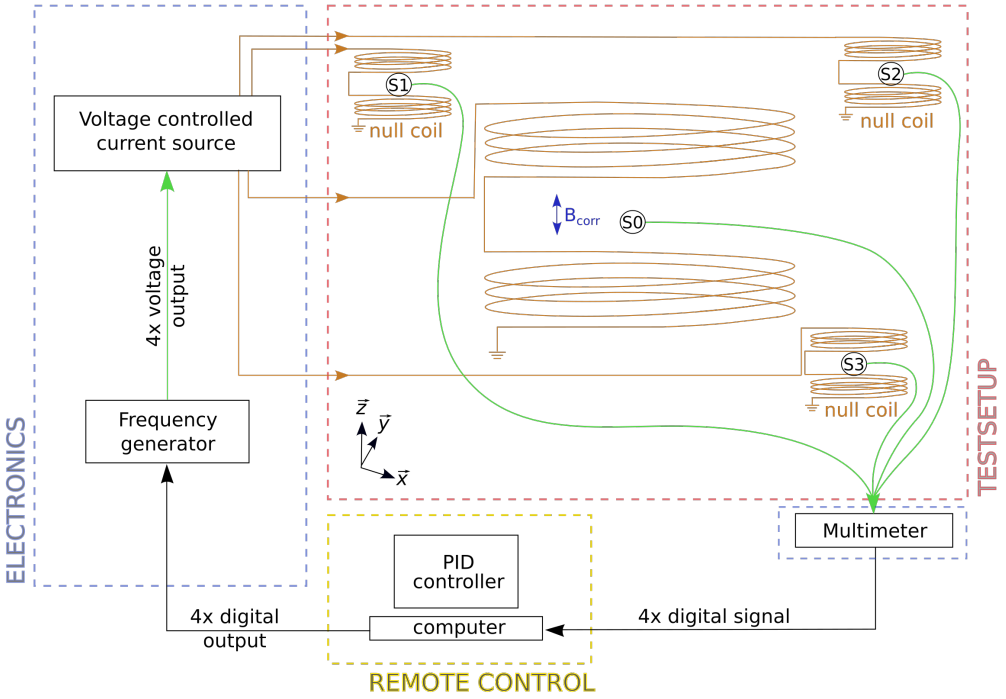

Figure 5.1: This schematic shows the main parts of the test setup for the active magnetic field stabilization system. The brown lines indicate a controlled current running through a wire/cable, the black lines indicate a digital signal that is being transmitted and the green lines represent a measurement of the voltage.

Secondly, information if the magnetic field changes are global. If the external magnetic stabilization system compensates local magnetic field variations at sensor location outside, while secondarily controlling the Helmholtz coils, it will be over- or undercorrecting the magnetic field fluctuations inside the Helmholtz coils [Stre 14]. Fig. 5.4 shows an example of such an undercorrection between 20h and 21h. To avoid this correction of local variations, there are three fluxgate magnetometers surrounding the Helmholtz coils. When comparing the magnetic field readout of the different sensors, it is possible to distinguish between local and global magnetic field changes.

The magnetic field at the center of a pair of Helmholtz coils can be calculated as:

$$B_H = \left(\frac{4}{5}\right)^{3/2} \frac{\mu_0 I N}{R} \ , \tag{5.3}$$

with μ_0 the permeability of free space, N the number of turns on each coil and R the radius of the coils. The scaling factor described by Eq. (5.2) is then calculated by the ratio of magnetic fields created by Helmholtz coils and null coils:

$$C = \frac{B_H}{B_{null}} \frac{N_{null}}{N_H} \frac{R}{r} \ , \tag{5.4}$$

with the number of turns N_H and N_{null} on Helmholtz and null coils, respectively, and the radii R and r for the Helmholtz and null coils, respectively. However, this calculation neglects the feedback from the

large Helmholtz coils' magnetic fringe field on the outside sensors. If the current running through the Helmholtz coils is adjusted, the fringe field increases or decreases. This change in magnetic field at the sensor position cannot be distinguished from an external source of magnetic field change, resulting in an overcorrection. The fringe field at the position of the sensors is proportional to the Helmholtz current. This allows the adjustment of the scaling factor to an effective scaling factor C_{eff} , since the external magnetic field and the magnetic feedback field of the Helmholtz coils are added together:

$$C_{eff} = C + C_{feedback} \ , \tag{5.5}$$

In order to determine C_{eff}, a robust method was needed that could measure the factor even if there was a magnet at the center of the Helmholtz coils, shielding the ion from small external magnetic field changes, instead of a sensitive fluxgate magnetometer with readout times of around 0.5 s. All external magnetic field changes that could be forced and would be strong enough to be measurable in the ions frequencies, even with the magnet's shielding, e.g. moving the heavy duty crane, are not global. Instead, an inverse approach was tested, in which the set point for the PID controller was changed to different values, mimicking the influence an external field change would have on the system. In order to calculate C_{eff}, each sensor, the outer as well as the sensor at the center of the Helmholtz coils, was equipped with its own PID controller, both simultaneously switching from one set point to the next, every couple of minutes. Fig. 5.2 shows the resulting magnetic field with the corresponding set points as well as the current applied to the coils, ascertained by the PID controllers.

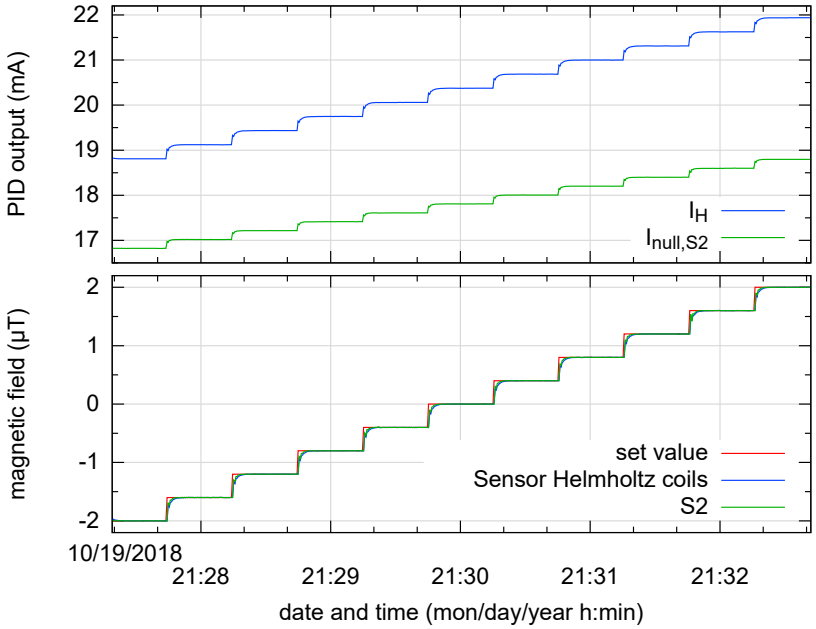

Figure 5.2: The figure shows the data of a C_{eff} measurement. The upper figure shows the PID-calculated currents necessary to reach the different magnetic field set points shown in the lower plot. More details are described in the text.

I_{null} and I_H can then be linearly fitted in order to obtain C_{eff} in addition to a constant offset due to the different absolute magnetic fields B_0 at the locations of the sensors. Fig. 5.3 shows the fit and the residuals of the measurement shown in Fig. 5.2.

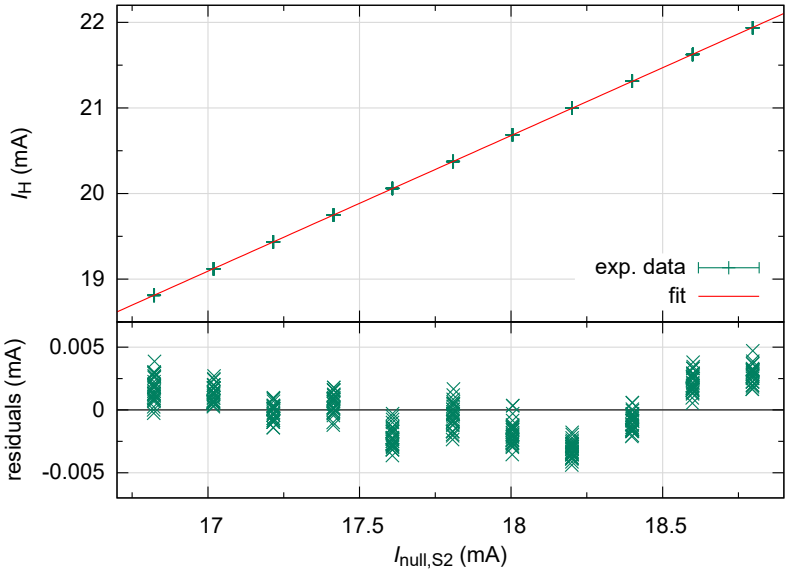

Figure 5.3: The figure shows a linear fit of the currents from the measurement shown in Fig. 5.2. Fit function: $I_H = C_{eff} \cdot I_{null,S2} + \text{offs.}$. The fit parameters were determined as $C_{eff} = 1.585(1)$ and offs. $= 7.8517(30)$ mA.

External stabilization test

After the scaling factor and offset were determined in a separate measurement, the external stabilization could be started. This external stabilization uses a PID controller to determine the current needed to stabilize the magnetic field at the position of sensor 2. This current is then applied to the null coils around sensor 2, via the frequency generator and voltage-controlled current source (see Fig. 5.1). In addition to this, the current is also applied to the large Helmholtz coils, but multiplied with the previously determined scaling factor $C_{eff} = 1.585$ and offseted by 7.8517 mA. In this scenario a sensor on the outside of the Helmholtz coils, i.e. sensor 2, is used to stabilize the magnetic field on the inside of the Helmholtz coils, i.e. future position of the Penning traps. Therefore, it is called an *external stabilization*. The results of the external stabilization are shown in Fig. 5.4. The stabilization system did manage to suppress the effect of the daily variation in the earth's magnetic field, which are the only truly global fluctuations at the PENTATRAP location. This improved the magnetic field stability during the day, as shown in Fig. 5.5a. However, the stabilization system increased the noise of the magnetic field, reducing the stability during the night (see Fig. 5.5b). This magnetic field noise seems to originate from the PID controlled current applied to the Helmholtz coils via a voltage-controlled current source which fluctuates slightly, creating

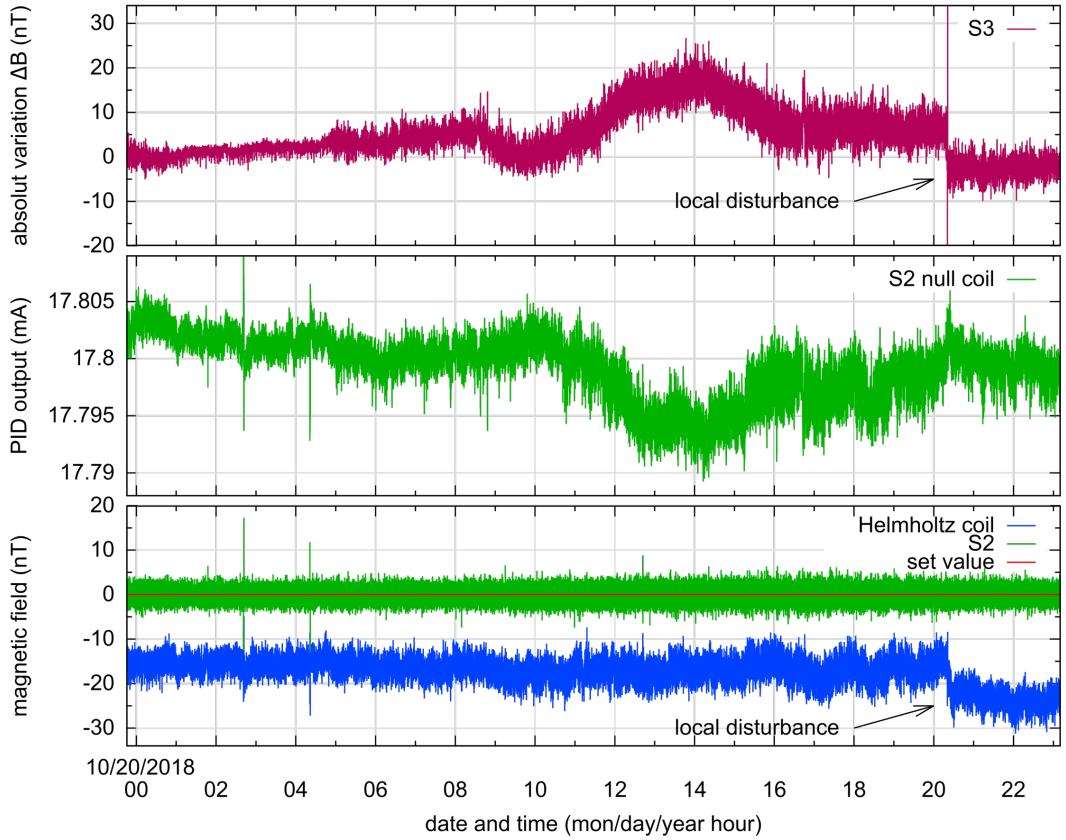

Figure 5.4: The figure shows a test measurement of a the magnetic field stabilization system with a stabilization via sensor 2 located on the outside of the Helmholtz coils. The upper plot shows the magnetic field not stabilized and measured with sensor 3 (for an overview of the test setup see Fig. 5.1). The middle plot shows the current output, determined by a PID controller in order to null the magnetic field at the position of sensor 2. The resulting stabilized magnetic field is shown in the lower plot. The magnetic field of the Helmholtz coils is indirectly stabilized by an external stabilization via S2. More information can be found in the text.

a jitter in the magnetic field. Therefore, the stability that can be reached with the stabilization system is limited by the stability of the current source.

For local magnetic field disturbances, the external stabilization needs to be corrected, as can be seen in Fig. 5.4. Furthermore, C_{eff} could not be definitively determined since the results of successive C_{eff} measurements did not agree within 3σ. This is most likely due to a changing C_{eff} every time something magnetic is moved in the vicinity of the setup or an experiment in the surrounding laboratories using strong magnets changes its magnetic field, e.g. the Heidelberg EBIT ramp up. This would mean, that C_{eff} needs to be determined repeatedly, i.e. before every new measurement.

In Fig. 5.4 one can see an offset of 20 nT in the magnetic field of the Helmholtz coils, originating from the long-term stability of the current source, i.e. the absolute current is creating an offset. Whereas

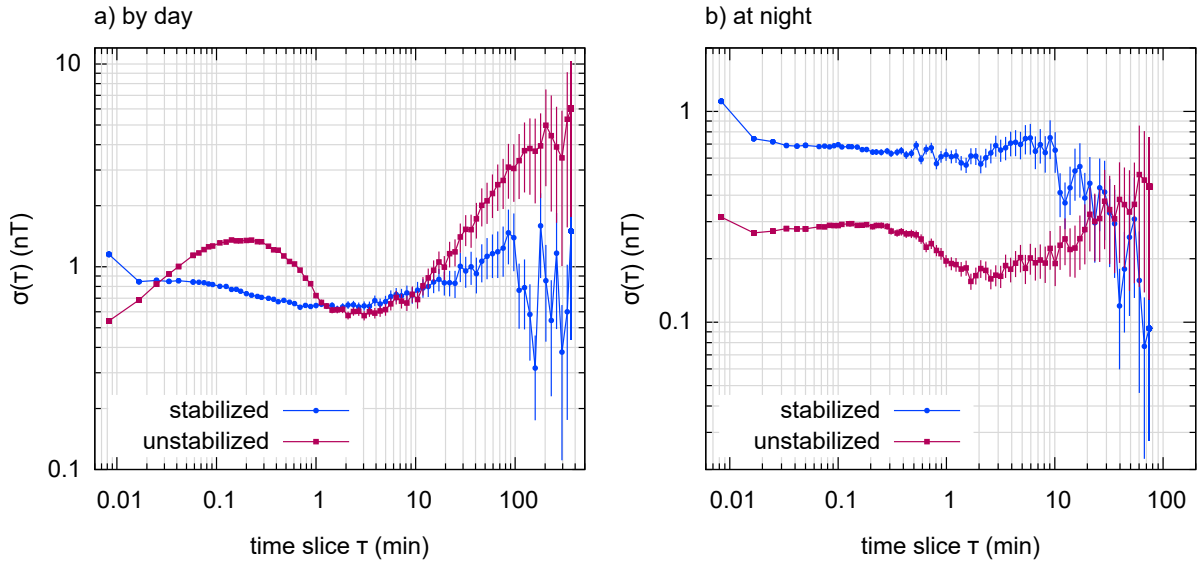

Figure 5.5: The figures show Allan Deviations with and without stabilization for a) during the day and b) during the night, i.e. between 1 a.m. and 5 a.m.. The underlying measurement can be seen in Fig. 5.4.

an offset of the magnetic field would not disturb the frequency measurements, there were also drifts of the magnetic field at the center of the Helmholtz coils visible in some of the test measurements. These magnetic field drifts, created by either the scaling factor changing over time or the long-term stability of the current source, need to be avoided, as they decrease the magnetic field stability.

The main difference to other Penning-trap experiments using an active stabilization system was the scale of fluctuations requiring stabilization. In the paper by R.S. Van Dyck from 1998 [Van 99], a stabilization system was described with a compensation factor of between 50 and 80, where the fluctuations of >100 nT over less than a minute originated from an electric trolley system nearby. The compensation factor describes the factor by which the magnetic stability is improved through the active stabilization system. This is not comparable to the global magnetic field changes of < 15 nT/h, that were the largest source of global magnetic field shifts at PENTATRAP (see Sec. 4.1). In order to stabilize these small changes in the magnetic field, a stabilization system would be needed with an even more precisely controllable current source and a faster readout of the magnetic field sensors, in order to reduce the magnetic field noise created by the magnetic field stabilization system. However, since these small global shifts in magnetic field do not limit our current precision, it was decided not to implement the active magnetic field stabilization system at PENTATRAP for now.

For future frequency measurements on ions which are more sensitive on magnetic field fluctuations, i.e. ions with a lower m/q (see Fig. 4.1), it would be advisable to measure only during the night when the earth's magnetic field fluctuations are smaller than the fluctuations during daylight and to monitor the magnetic field closely to exclude data taken during unexpected large magnetic field jumps.

5.2 Temperature stabilization system

The temperature in the laboratory is stabilized by an air conditioning unit by Siemens [Siem 10]. Since the last detailed temperature measurements using this air-conditioning system were taken about 10 years ago, several changes on the experiment and laboratory have been made in the meantime. Therefore, an optimization of parameters and a general test of the system was necessary. Changes on the experiment and laboratory included:

- The housing of the magnet as a secondary temperature stabilized volume has been removed, since it made work on the magnet, like filling liquid helium, unnecessarily complicated.
- The air heaters for stabilization have been removed.
- Electrical components in the laboratory have been set up, e.g. the ultra-stable voltage source StaReP, which now contribute as additional heat sources [Böh 16].
- The hole in the ceiling where the beamline enters has been enlarged.

The stabilization system is made up of two separately cooled streams of supply air that can be interchanged, as shown in Fig. 5.6. The dual system is meant to prevent failure of the air supply and is

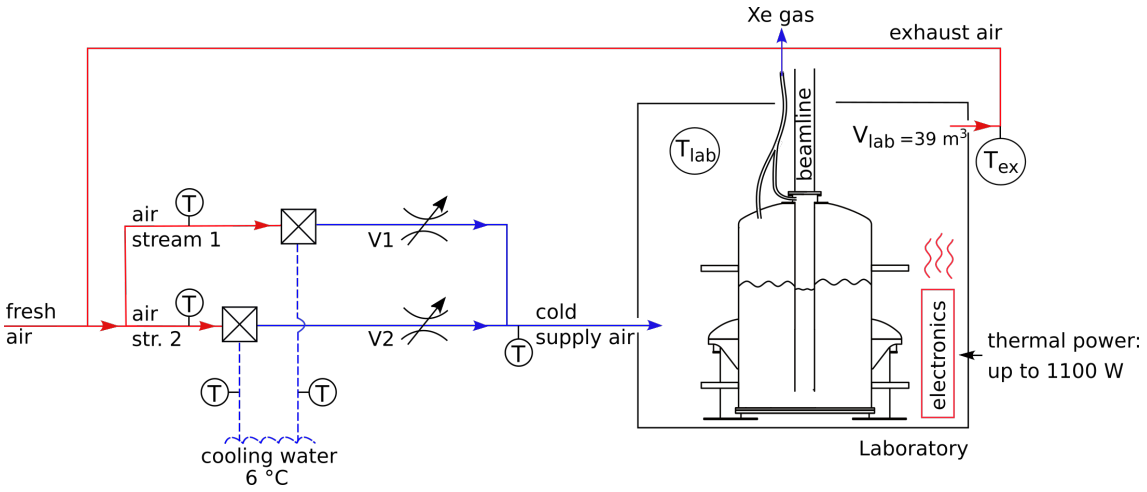

Figure 5.6: Schematic overview of the ventilation-controlled temperature stabilization system at PENTATRAP. The warm streams of air are colored in red, while blue symbolizes cold air (solid line) and cold water (dashed line). The system aims to stabilize the laboratory temperature T_{lab} by stabilizing the exhaust air temperature T_{ex} to a chosen set point, e.g. 18 °C. Air streams 1 and 2 are interchangeable to ensure a continuous fresh air supply in case of pump or valve failure.

switched every couple of days by opening valve V1 and closing valve V2 or vice versa. Switching the two supply air streams makes sure, that none of the valves or pumps breaks during the long time between usage. The cold air is then gradually released into the laboratory until the temperature T_{ex} reaches a

certain set point. The warm exhaust air is returned to the supply side of the system and used again by mixing it with fresh air and cooling it once more with the 6 °C cooling water (circular air operation).

5.2.1 Optimization of the temperature stability

Originally determined by *Siemens*, the temperature stability was <0.1 °C over one day [Siem 10]. However, due to the changes to the system described above, the stability was much worse (see Fig. 5.7).

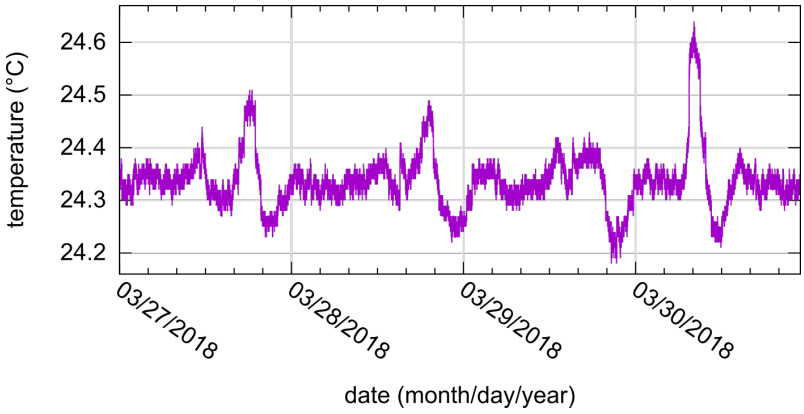

Figure 5.7: This plot shows the temperature stability before the optimization process.

In order to get close to the original value, the following steps showed positive results:

1. Filling the hole (ca. 0.4 m^2) in the ceiling of the laboratory for the beamline with insulating material to stop uncontrolled air flow and temperature loss.
2. Lowering the temperature set point, since without heaters the only controllable parameter of the system is the amount of cold air flowing through the laboratory, therefore a lower temperature set point can be reached faster, resulting in a better stability.
3. Lowering the supply air temperature to speed up the cooling process.
4. Re-optimizing the controller parameters with the help from the people of the utilities management.
5. Less frequent switches of air stream 1 and 2 (every other week) since each valve switch causes a temporary increase of temperature by more than 1 °C. And then finally stopping the air stream switches altogether since air stream 1 seems unable to produce a stable temperature. A temperature oscillation with a period of several hours and an amplitude of 0.2 °C kept arising.
6. Waiting $\sim$ 4 hours after entering the laboratory to start a frequency measurement, so the temperature can settle to the chosen set point.

After theses steps have been carried out, the temperature stability lies now below 0.02 °C over half an hour, see Fig. 5.8, depending on the time scale and location of the sensor in the laboratory.

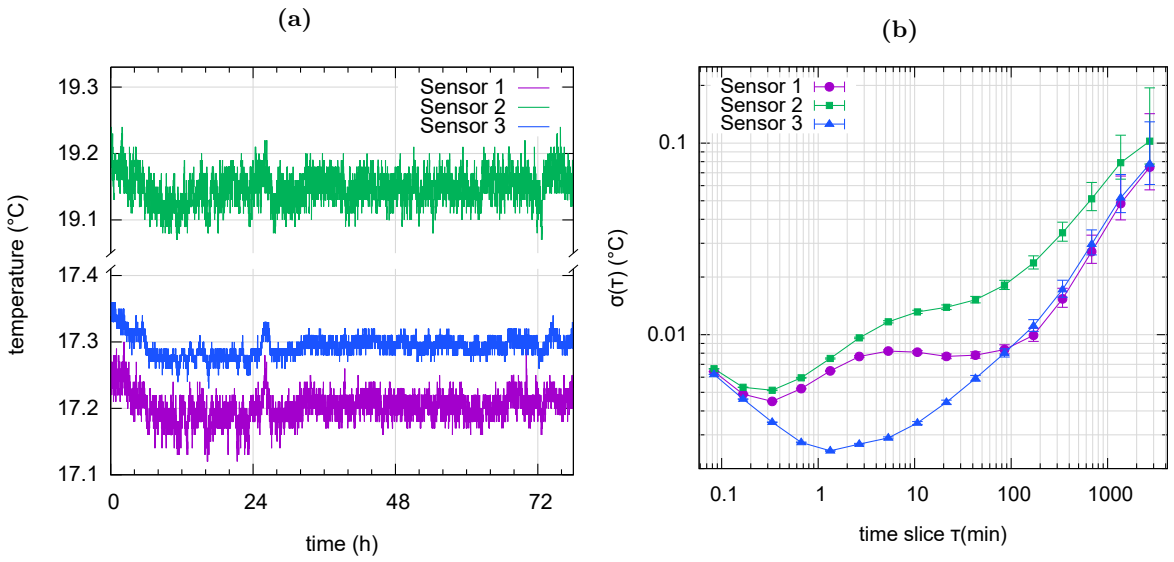

Figure 5.8: Temperature behaviour with the optimized stabilization system. For sensor location see Fig. 3.5. Figure a) shows typical fluctuations while the laboratory door stays closed (in Dec. 2018). Sensor 2 is located in the rack for the electronics, so it measures a higher temperature due to the heat load of the electronic components close to it. b) shows the resulting Allan Deviation for the three sensors, calculated with the software *AlaVar 5.2* [Alam]. The BMP280 sensors only have a resolution of 0.01 °C, so stabilities shown here of below 0.01 °C are slightly underestimated.

StaReP housing

One of the most temperature-sensitive components in the setup is the ultra-stable voltage source StaReP [Böh 16]. In order to avoid wind chills from the cold supply air and thereby improve the short-term temperature stability of the voltage reference and channels, an insulating housing of StaReP was proposed and tested. However, the tests showed that due to the high heat load of StaReP itself, the temperature inside the housing rose to >35 °C. StaReP's heat load is made up of 6 W from the controller, 3.48 W from each channel and 15 W from the reference module, resulting in a combined heat load of approx. 110 W. The temperature stability inside the housing was similar to the stability before the housing, however after temperature changes in the lab, e.g. after filling liquid helium or opening the door, it took 7 hours to stabilize again. Due to the long waiting period before a frequency measurement could be started, i.e. until the StaReP temperature was stable again, and because the voltage reference tends to get less stable at high temperatures, it was decided to remove the housing again.

5.3 Helium-level and pressure stabilization

As seen in the measurements described in Sec. 4.3, a temperature stabilization of the cold bore is necessary to make the cyclotron frequency of the stored ion less dependent on external pressure variations and to

keep the helium level in the cold bore constant, in spite of the helium evaporation (details will be given below). The temperature, as described before in Eq. (4.6), depends on pressure and the liquid-helium level. In order to stabilize the temperature it is therefore necessary to keep the helium level and the pressure in the cold bore constant.

At PENTATRAP the helium dewar is divided into two compartments: the cold bore containing the traps and detection systems and the outer reservoir with the superconducting coils of the magnet. The two volumes are connected to each other through capillaries below the liquid-helium surface, at the bottom of the cold bore (see Fig. 5.9). This setup makes it possible to keep helium level and pressure constant in one of the tanks, by controlling the gas flow of evaporated helium out of both tanks. The pressure in the cold bore is controlled by adjusting the flow of evaporated helium through its own outlet. The helium level is kept constant by adjusting the flow out of the magnet's reservoir, thereby changing the pressure, which draws more helium out of the cold bore or pushes more helium into it.

5.3.1 Experimental implementation of the pressure and helium-level stabilization system

The pressure and helium-level stabilization system described in this chapter and tested during this thesis was first developed and built in its original form for PENTATRAP by [Risc 14] and [Böh 15] and based on the concept of [Stre 14]. To keep pressure and helium-level constant and thereby T_{evap}, two main sensors are necessary - a level and a pressure sensor. They have to run in a continuous mode to feed the necessary information to the PID controller which then adjusts the flow controllers controlling the gas flow of the continuous evaporation of helium from both the cold bore and the reservoir. In Fig. 5.9 an overview of the system is given.

Relative pressure sensor and absolute pressure reference

The pressure in the cold bore is measured by a 120AD pressure transducer connected to a PR4000B device by *MKS-Instruments* [MKS a, MKS b]. The 120AD sensor measures the pressure relative to the absolute pressure reference (APR) [Stre 14]. In order be able to stabilize the pressure, the set value has to be high enough above atmospheric pressure, so daily variations in ambient air pressure still allow a pressure control by controlling the outflow of evaporated helium. If the pressure set value is chosen too low and the barometric air pressure rises above the set value, the pressure in the cold bore can no longer reach the set value, which causes a system failure. Since the 120AD pressure sensor has a resolution of 10^{-6} over the full range, the APR pressure is filled to an absolute pressure of $\sim$1015 hPa, making it possible to stabilize to the relative pressure of 0 hPa, using the highest resolution of the sensor.

Relative pressure sensor and APR pressure stability

The achievable pressure stability in the cold bore lies below 0.02 hPa peak to peak, see Fig. 5.10(d), according to the relative pressure readout. However, this relative measurement cannot measure drifts

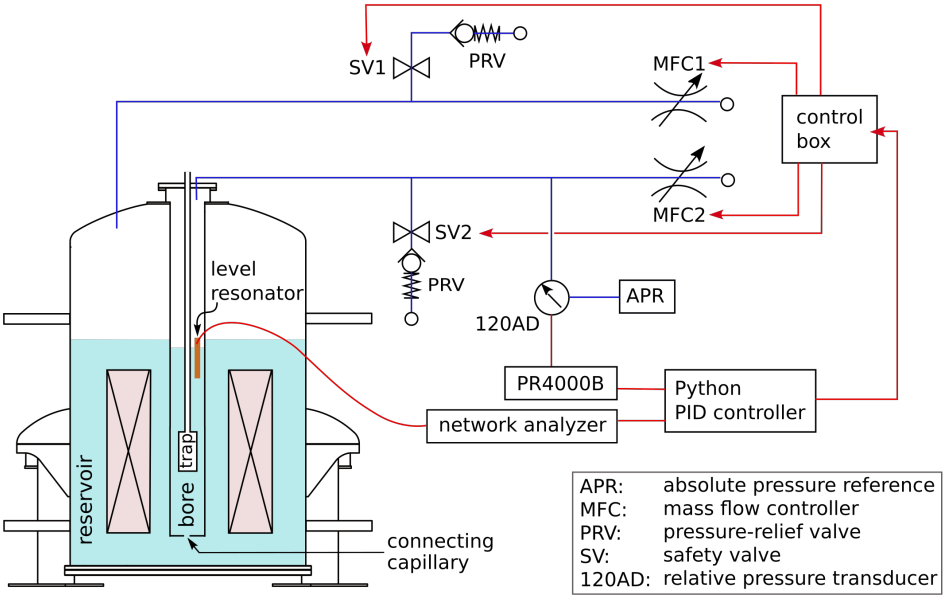

Figure 5.9: Overview of the experimental implementation of the helium-level and bore-pressure stabilization system at PENTATRAP. To the left a schematic of the helium dewar with the two compartments and the dispersed magnet and traps can be seen. The blue lines signify gas pipes leading the vaporized helium to the outside. The red lines are electronic connections necessary for read/write functions and control of the gas flow. Further information can be found in the text.

of the pressure inside the APR. Even though being enclosed in a thick layer of thermally insulating material (Styrofoam) and having its own thermal mass, the APR pressure fluctuates with temperature. The temperature dependence was investigated to be approximately:

$$\Delta p = (1.5 \pm 0.5)\ \text{hPa/K} \cdot \Delta T\ , \tag{5.6}$$

by comparing the relative pressure measured by the 120AD sensor and APR to an absolute pressure sensor type BMP280. The drift with temperature of the APR can be seen in the absolute pressure data in Fig. 5.10(d) when comparing it to the laboratory temperature in Fig. 5.10(e). In addition to this slow drift with temperature, the sinking absolute pressure behaviour after filling the APR implies the possibility of a leak in the APR, its connection to the pressure sensor or the sensor itself. To improve the pressure stability of the system without these drifts, a modified setup is planned, not using the APR anymore, instead it is based on a new absolute pressure sensor 6000-23A by *Althen* with an accuracy of 0.01% and a resolution of $1 \cdot 10^{-8}$ [Alth 19].

Level sensor

For a quickly reacting level stabilization system a sensor is needed that can be run in a continuous mode while not having too big of a heat load which would boil off and waste a lot of helium. This would shorten the liquid-helium holding time in the magnet, which has to be avoided under any circumstances.

Making use of the fact that liquid helium has a different permittivity than helium in its gaseous form, an LC circuit fulfills these requirements. By hanging a long capacitor in the cold bore, the capacitance will depend on the liquid-helium level, as long as it is not completely immersed in liquid helium or only surrounded by helium gas [Risc 14]:

$$C(l) = \frac{2\pi\epsilon_0}{\ln \frac{R_2}{R_1}}(\epsilon_l l + \epsilon_g(H - l)) \ , \tag{5.7}$$

with C being the capacitance, R_1 the inner and R_2 the outer radius of the cylinder, H the complete height of the cylinder, l the level (height) of the liquid helium and ϵ_l/ϵ_g the permittivity of the liquid and gaseous helium. For measuring the changes in the capacitance, an inductance L is added, creating an LC circuit with a resonance frequency at:

$$\omega_0(l) = \frac{1}{\sqrt{L \cdot C(l)}} \ . \tag{5.8}$$

When assuming a constant inductance, the resonance frequency of the LC circuit is level dependent. The higher the frequency the lower the helium level. The resonator used inside PENTATRAP has a length of 99.2 mm, a level sensitivity of (0.25 ± 0.05) μm per Hz and is located around 23 cm above the trap chamber [Risc 14]. The achievable level stability can be seen in Fig. 5.10(c).

Flow control

The stabilization system uses two Bronkhorst F-201EV mass flow controllers (MFCs) [Bron], which get controlled by two separate PID controllers. The first PID controller uses the helium level as an input value to control MFC1. The second PID controller receives its input value from the pressure sensor and controls MFC2. The python scripts running the PID controllers sends the output to the control box, which is then adjusting the MFCs.

Pressure-relief valves

To make sure there won't be any pressure build-up in case of a script failure, the control box will open the valves if it does not get a script response at least every 10 seconds. If there is an error message or no return message, e.g. in the case of a power failure, the hydraulic safety valves SV1 and SV2 will open, clearing the way to the mechanical pressure-relief valves (PRV1 and PRV2). If the valves did not open, the temperature inside the reservoirs would rise and increase the helium consumption.

5.4 Cyclotron frequency measurements with stabilization

In the following, a cyclotron frequency measurement of a single $^{187}Re^{29+}$ ion is presented in Fig. 5.10(a)/(b), with the simultaneous measurement of the stabilized helium level (c), pressure in the cold bore relative to the APR (d), absolute pressure in the cold bore (e), temperature in the laboratory (f), absolute ambient pressure (f), and external magnetic field (g). The measurement was carried out as part of the energy

level determination of metastable states in $^{187}Re^{29+}$ ions at PENTATRAP [Schu]. Due to the length of the measurement it was particularly suitable for a comparison to all environmental data currently being logged at PENTATRAP. The measurement shown in Fig. 5.10(a) and (b) covered three full measurement cycles which were each made up of a phase-unwrapping measurement in the beginning (see hour-long horizontal gaps in the data) and 25 cyclotron determination measurements, before the ions were lost. Each of the ν_c-determination measurements are an average over 10 combined PnP and axial measurements. Fig. 5.10(a) and (b) show these averaged cyclotron frequencies in traps 2 and 3. A cyclotron frequency offset between position 1 and 2 is visible. The offset was discovered to be due to the different electronic states the ions were in. While all the ions had the same charge state, some of the ions were produced in an electronically excited, metastable state (for more information on this see [Schu]). The cyclotron frequencies in both traps and of both ions are linearly decreasing for the first two thirds of the measurement. This drift is on the scale of $2 \cdot 10^{-10}$/h. Since the cyclotron frequencies have been decreasing monotonously, since the pressure and level stabilization system has been built in, this drift is most likely due to the flux-creep effect in PENTATRAP's magnet, known to exist in many other systems as well [Mukh 08]. The flux-creep effect describes an effect where a superconducting magnet loses its field magnitude over time (this is a linear effect over weeks) [Ande 62]. This gives an estimate of the scale of the loss of magnetic field due to the flux-creep effect of $2 \cdot 10^{-10}$/h. Towards the last third of the measurement, the cyclotron frequency (especially in trap 2) seems to stop decreasing. This effect might be due to the absolute bore pressure and/or the external magnetic field variation. External magnetic field changes of up to 100 nT as seen in plot (g) can have a relative effect on the cyclotron frequency of up to ($3 \cdot 10^{-10}$/100 nT). These strong fluctuations are due to the workday at the experimental hall (see Fig. 4.4d). The difference between May 26, which was a Sunday, and May 27, which was a Monday and normal workday is clearly visible in Fig. 5.10(g). External magnetic field shifts should have almost the same effect on both traps, or a slightly smaller effect on trap 2, due to the shielding factors listed in Sec. 4.1.3. However, the effect is more prominently visible in trap 2 and the frequency stays stable instead of fluctuating with the external magnetic field, so the more likely reason or larger contribution to the flattening curve is the APR pressure drift. The pressure of the APR (see Fig. 5.10(e)) is rising due to the increasing external temperature (see Eq. (5.6)). When taking the flattening of the linear frequency drift of the flux-creep effect into account, an upper limit to the temperature dependence of the cyclotron frequency due to the temperature dependence of the APR, i.e. the pressure stabilization system, can be estimated: $8 \cdot 10^{-9}$/K.

When the cyclotron frequency in both traps behaves the same, the possibility exists to use the cancellation method described in Sec. 3.4. When the new absolute pressure sensor for the pressure stabilization system will be built in, this drift should disappear, opening up a higher precision on this new measurement method. Besides the flattening in the frequencies towards the end of the measurement, all other environmental effects seem to be suppressed by the combination of temperature, helium-level and bore-pressure stabilization systems.

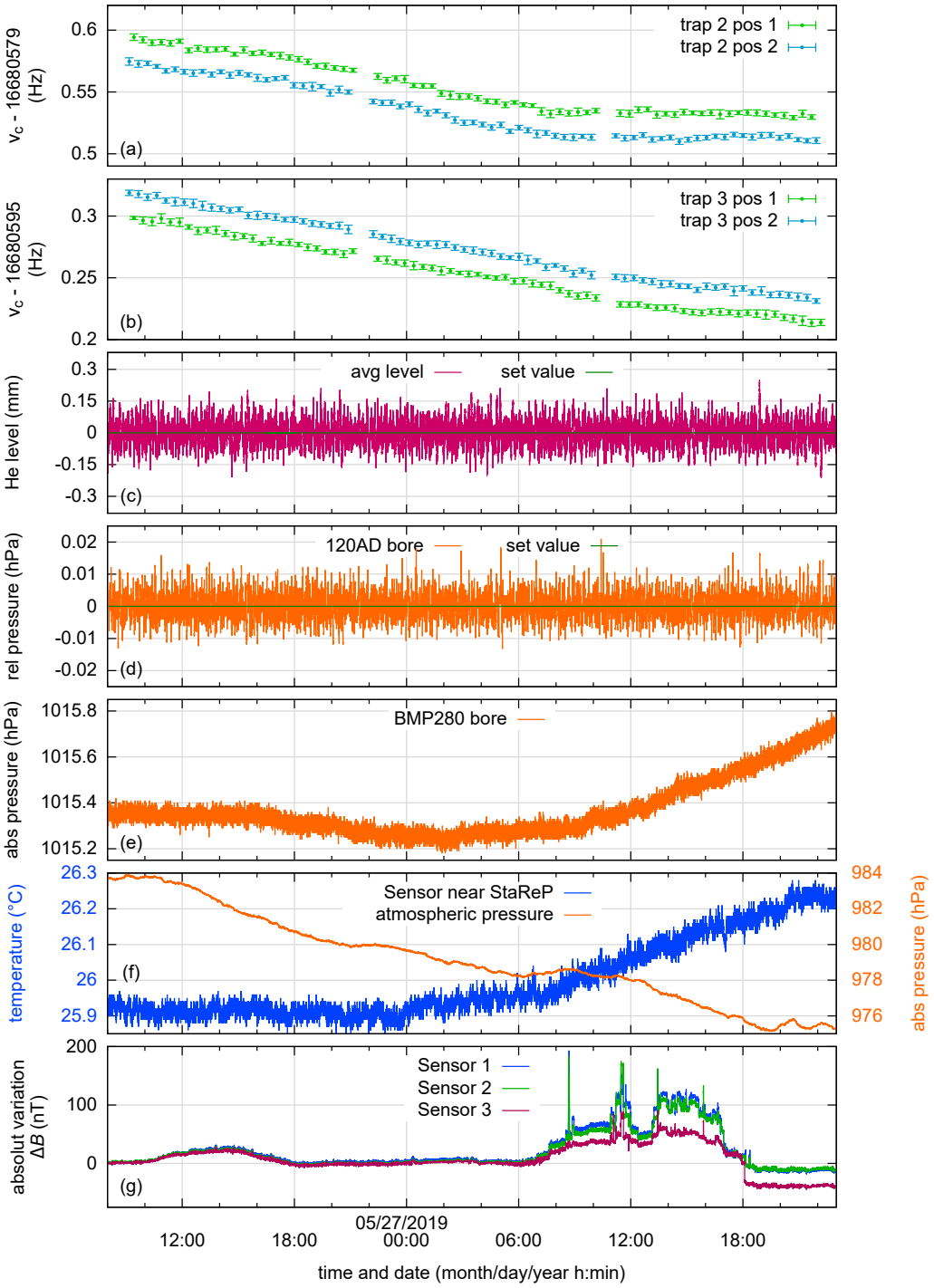

Figure 5.10: This figure shows an overview of a frequency measurement of $^{187}Re^{29+}$ ions measured in comparison to the environmental data. The frequency data was analyzed as part of the PhD thesis work of R.X. Schüßler [Schu]. For details see text.

Chapter 6

Summary and Outlook

The mass spectrometer PENTATRAP aims at determining the mass ratios of heavy, highly-charged ions to a relative uncertainty in the range of 10^{-12}, with possible applications in neutrino physics and in tests of fundamental theories like special relativity. While relative uncertainties of 10^{-11} are now routinely reached at PENTATRAP [Risc 18], this thesis was aimed at identifying and lowering the systematic uncertainties in order to get closer to the desired precision. In the framework of this thesis, the influence that environmental parameters have on an ion in a Penning trap have been investigated and stabilization systems for the relevant environmental parameters have been tested accordingly.

External magnetic field fluctuations influence the magnetic trapping field of the Penning traps. The effect is suppressed by the shielding factor of PENTATRAP's superconducting magnet. The determination of the shielding factor resulted in a value of $S \approx 50$ for traps 2 and 3. An active magnetic field stabilization system using Helmholtz coils was tested, however, the small and slow global magnetic field fluctuations of up to < 15 nT/h of the earth's magnetic field, that could be counteracted with this stabilization system, are not limiting the relative precision in the range of 10^{-12} of the frequency-ratio measurements. While a stabilization of the global magnetic field changes during the day has been achieved, the larger local changes caused by e.g. the ferromagnetic heavy duty crane, could not be counteracted. Furthermore, due to the stability of the current source, the stability of the external magnetic field during the night was worsened by the stabilization system. Moreover, the scaling factor needed for the external control of the Helmholtz coils was changing over time and therefore could not be clearly determined. It was decided that, for now, the active magnetic field stabilization system will not be used at PENTATRAP. Instead, measurements with a required relative precision of below 10^{-11} or measurements on ions which are more sensitive to the external magnetic field changes, i.e. ions of lower m/q, are carried out at night or on weekends when sources of larger magnetic field disturbances are at a minimum.

The temperature in the laboratory influences StaReP, the ultra-stable voltage source for the trapping potentials [Böh 15]. While StaReP's new voltage reference was found to be mostly temperature-stable, with a relative dependence of below $1 \cdot 10^{-8}$/K, the temperature stabilities of the 25 channels, e.g. channel 24: $\sim 2 \cdot 10^{-5}$/K, add up to an overall temperature dependence of the axial frequency of $\sim 10^{-6}$/K. In

order to keep the trapping voltages as stable as possible, the air-conditioning system at PENTATRAP was optimized, resulting in a temperature stability of below 20 mK/h and around 100 mK/d. With this improved stability, the temperature dependence of the trapping potentials allows measurements to a relative frequency uncertainty in the range of 10^{-12}. With highly charged chlorine ions, e.g. $^{35}Cl^{+15}$, the precision of the mass-ratio measurement for the test of $E = mc^2$, described in Chap. 1, should not be limited by the systematic uncertainty due to the temperature dependence of the trapping potentials. It has been found that the ambient pressure stability limits the cyclotron-frequency precision by changing the magnetic susceptibility of the trap materials. In order to reduce this effect by stabilizing the temperature inside the cold bore of the magnet, a helium-level and pressure stabilization system has been installed and tested successfully. Since then, the cyclotron frequency of the stored ion no longer fluctuates with the ambient pressure. While the system was very effective with respect to the stabilization against ambient pressure, the absolute pressure reference needed for the relative pressure sensor is fluctuating with temperature. Thereby, the pressure in the cold bore was not stabilized to an absolute pressure set value, which resulted in a relative cyclotron frequency drift of max. $8 \cdot 10^{-9}$/K. An update of the pressure stabilization system with an absolute pressure sensor should reduce this effect and further improve the pressure stability and thereby temperature stability in the cold bore. With the improved temperature stability and the use of the helium-level and pressure stabilization system, the newest mass-ratio measurements of two $^{187}Re^{29+}$ ions yielded a relative precision of $8 \cdot 10^{-12}$ [Schu].

Environmental parameters influencing PENTATRAP will have to be continuously monitored. The magnetic field fluctuations created by surrounding experiments during working days, reduces the precision of the cyclotron-frequency measurement. While measuring at night and on weekends mostly avoids the cyclotron frequency shifts, the statistics could be increased when measuring during days and nights. In order to increase the statistics, an option is to monitor the magnetic field during working days and exclude data if the magnetic field changes get larger than the calculated limits for the different ion species. In the future, the stabilization system with the Helmholtz coils could be tested again with a more stable current supply and a faster readout system.

The temperature stabilization system has been optimized for the current state of the experiment but will have to be kept updated with any changes in the laboratory. The influence of the temperature stability is expected to decrease once the new absolute pressure sensor will be installed in the helium-level and pressure stabilization system. This absolute sensor will no longer need a temperature dependent absolute pressure reference. With this improved setup and longer measurement times it should be possible to reach a relative precision of the mass-ratio measurement of only a few parts of 10^{-12}.

Appendix A

Environmental influences: additional data

A.1 Magnetic field on a Sunday night

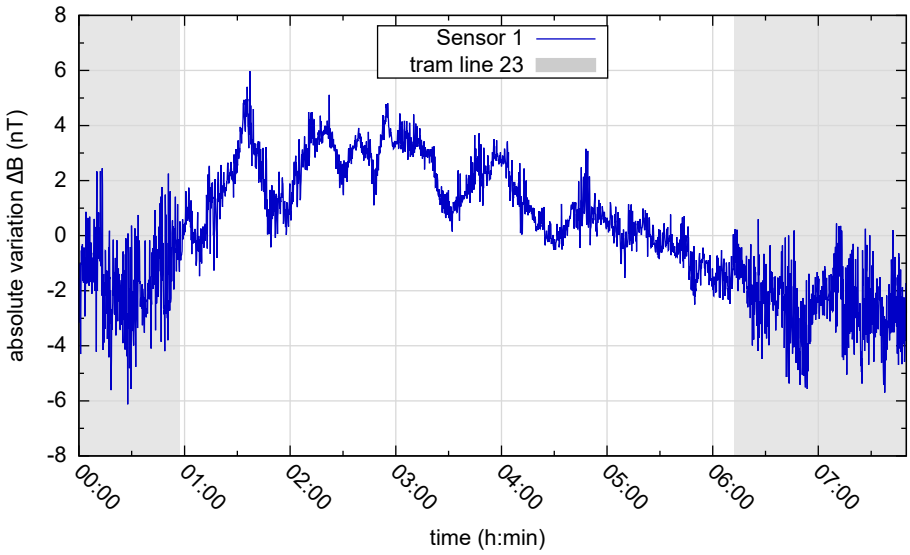

Figure A.1: The external magnetic field variation in the laboratory during a sunday night May 5, 2019 is shown. Amplitude changes are visible in the fast fluctuations. The shaded regions indicate when the tram line is running on the sunday/public holiday schedule.

A.2 Temperature dependence StaReP

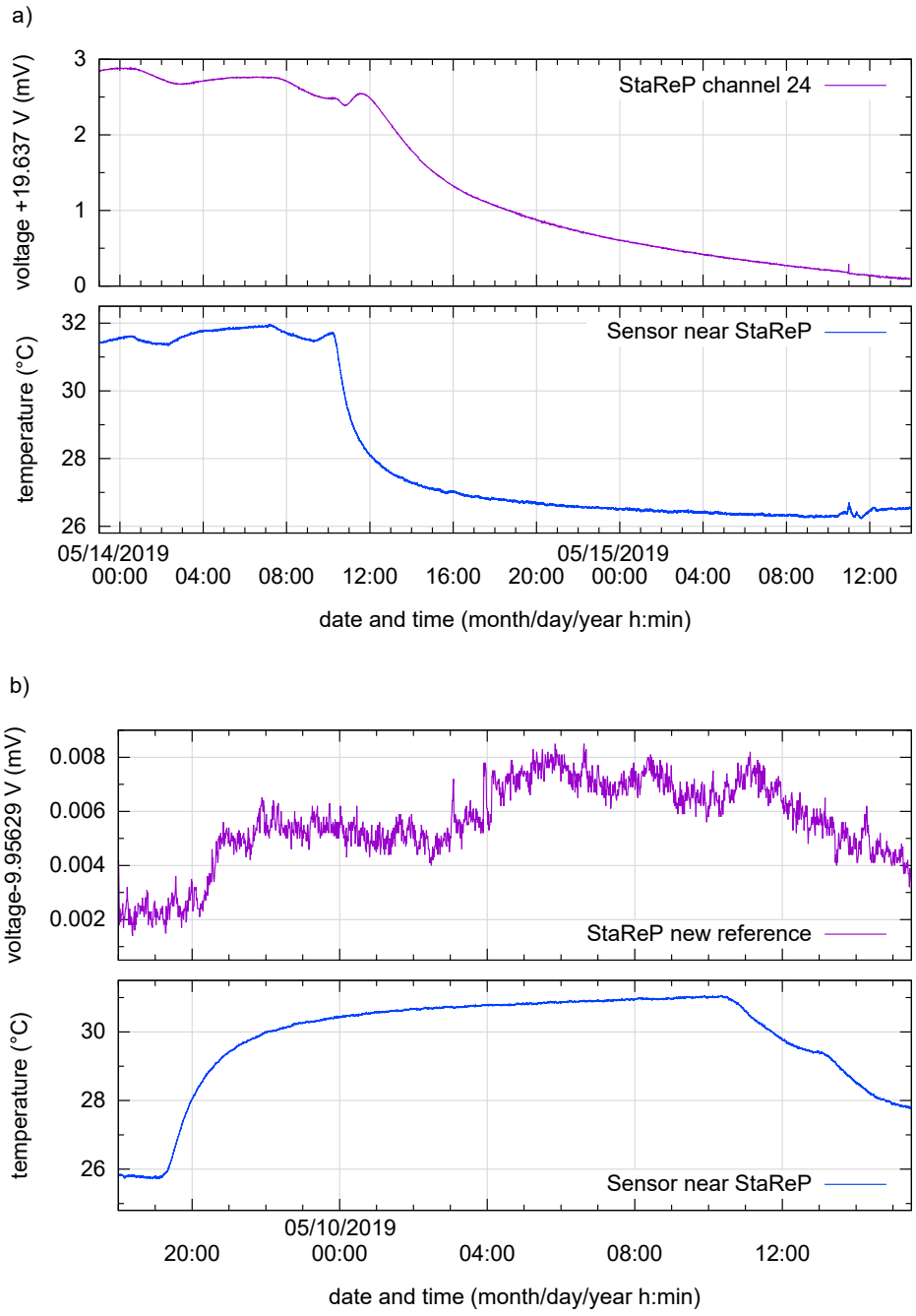

Figure A.2: This figure shows the temperature dependence of StaReP's components a) channel 24 and b) the new temperature stabilized voltage reference. The output voltages were measured with the reference multimeter 8508A by *Fluke* [Fluk]. The multimeter was exposed to the same temperature changes during the measurement, though its temperature coefficient is neglectable compared to the measured shift.

A.3 Pressure-correlated cyclotron frequency drifts

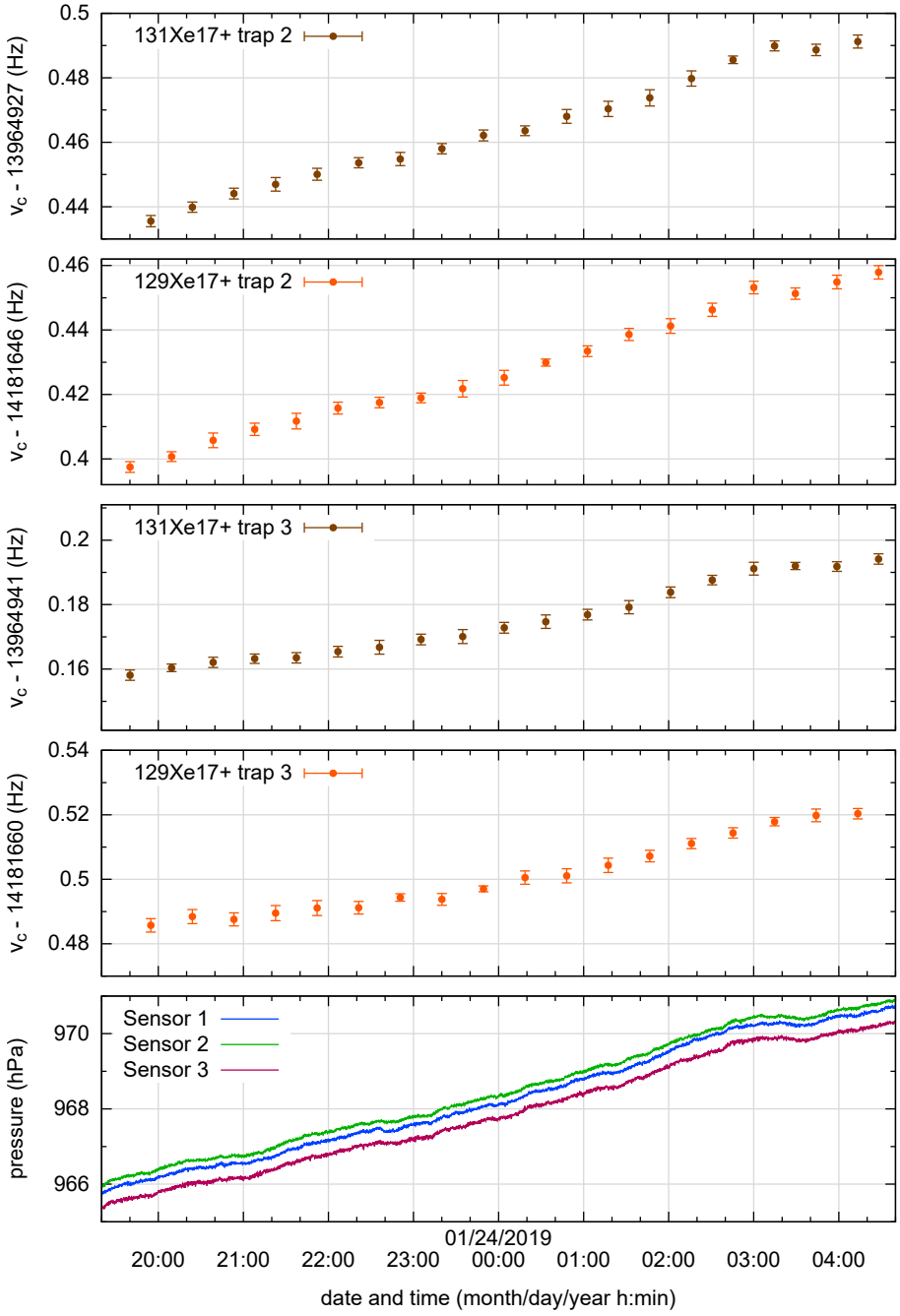

Figure A.3: The figure shows the cyclotron frequencies of a $^{129}Xe^{17+}$ and a $^{131}Xe^{17+}$ ion in traps 2 and 3 in comparison to the ambient pressure prior to the installation of the helium-level and bore-pressure stabilization system. Both ions and both traps show the same trends as the ambient pressure, with a smaller amplitude of the drift in trap 3 than in trap 2.

Bibliography

[Alam] Alamath. "Allan Deviation calculator software AlaVar5.2". `http://www.alamath.com/alavar/`. Accessed: Mar, 2019.

[Alth 19] Althen. "Paroscientific high-precision pressure standard". personal communication, May 2019.

[Ande 62] P. W. Anderson. "Theory of Flux Creep in Hard Superconductors". *Phys. Rev. Lett.*, Vol. 9, pp. 309–311, Oct 1962.

[Apex] Apex-Microtechnology. "VRE102 precision voltage reference". `https://www.apexanalog.com/resources/products/vre102u.pdf`. Accessed: Jun, 2019.

[Bosc] Bosch. "BMP280 digital pressure sensor". `https://cdn-shop.adafruit.com/datasheets/BST-BMP280-DS001-11.pdf`. Accessed: September, 2018.

[Bron] Bronkhorst. "LOW-ΔP-FLOW F-201EV Mass Flow Controller". `https://www.bronkhorst.com/int/products/gas-flow/low-p-flow/f-201ev/`. Accessed: May, 2019.

[Brow 86] L. S. Brown and G. Gabrielse. "Geonium theory: Physics of a single electron or ion in a Penning trap". *Rev. Mod. Phys.*, Vol. 58, pp. 233–311, Jan 1986.

[Böh 15] C. Böhm. *High-precision mass measurements of neutron-deficient Tl isotopes at ISOLTRAP and the development of an ultra-stable voltage source for the PENTATRAP experiment.* PhD thesis, Ruprecht-Karls-Universität Heidelberg, 2015.

[Böh 16] C. Böhm *et al.* "An ultra-stable voltage source for precision Penning-trap experiments". *Nuclear Instruments and Methods in Physics Research Section A: Accelerators, Spectrometers, Detectors and Associated Equipment*, Vol. 828, pp. 125 – 131, 2016.

[Chit 17] G. Chitarin, D. Aprile, M. Brombin, N. Marconato, and L. Svensson. "Feasibility study of a flux-gate magnetic field sensor suitable for ITER neutral beam injectors". *Fusion Engineering and Design*, Vol. 123, pp. 412 – 416, 2017.

[Corn 89] E. A. Cornell, R. M. Weisskoff, K. R. Boyce, R. W. Flanagan, G. P. Lafyatis, and D. E. Pritchard. "Single-ion cyclotron resonance measurement of $M(CO^+)/M(N_2^+)$". *Phys. Rev. Lett.*, Vol. 63, No. 16, pp. 1674–1677, Oct 1989.

[Cres 04] J. R. Crespo López-Urrutia *et al.* "Progress at the Heidelberg EBIT". *Journal of Physics: Conference Series*, Vol. 2, pp. 42–51, Jan 2004.

[Door 18] M. Door. *New control system and first trap characterization measurements at the high-precision Penning-trap mass spectrometer PENTATRAP.* Master's thesis, Ruprecht-Karls-Universität Heidelberg, 2018.

[Dorr 18] H. Dorrer *et al.* "Production, isolation and characterization of radiochemically pure ^{163}Ho samples for the ECHo-project". *Radiochimica Acta*, Vol. 106, No. 7, pp. 535–547, Mar 2018.

[Dör 15] A. Dörr. *PENTATRAP: A novel Penning-trap system for high-precision mass measurements.* PhD thesis, Ruprecht-Karls-Universität Heidelberg, 2015.

[Fluk] Fluke. "8.5 Digit Reference Multimeter, 8508A". `https://eu.flukecal.com/de/products/electrical-calibration/bench-multimeters/referenzmultimeter-8508a-85-digits?quicktabs_product_details=4`. Accessed: May, 2019.

[Gabr 88] G. Gabrielse and J. Tan. "Self-shielding superconducting solenoid systems". *Journal of Applied Physics*, Vol. 63, No. 10, pp. 5143–5148, 1988.

[Gast 17] L. Gastaldo *et al.* "The electron capture in ^{163}Ho experiment – ECHo". *The European Physical Journal Special Topics*, Vol. 226, No. 8, pp. 1623–1694, Jun 2017.

[Huan 17] W. Huang, A. G., M. Wang, F. Kondev, S. Naimi, and X. Xu. "The AME2016 atomic mass evaluation". *Chinese Physics C*, Vol. 41, No. 3, p. 03002, 02 2017.

[Hurd 66] C. Hurd. "A magnetic susceptibility apparatus for weakly magnetic metals, and the susceptibility of pure copper in the range 6–300° K". *Cryogenics*, Vol. 6, pp. 264–269, 10 1966.

[Jeff 93] S. R. Jefferts, T. Heavner, P. Hayes, and G. H. Dunn. "Superconducting resonator and a cryogenic GaAs field-effect transistor amplifier as a single-ion detection system". *Review of Scientific Instruments*, Vol. 64, No. 3, pp. 737–740, 1993.

[Kess 01] E. G. Kessler, M. S. Dewey, R. D. Deslattes, A. Henins, H. G. Börner, M. Jentschel, and H. Lehmann. "The GAMS4 flat crystal facility". *Nuclear Instruments and Methods in Physics Research A*, Vol. 457, pp. 187–202, Jan. 2001.

[Kett 14] J. Ketter, T. Eronen, M. Höcker, S. Streubel, and K. Blaum. "First-order perturbative calculation of the frequency-shifts caused by static cylindrically-symmetric electric and magnetic imperfections of a Penning trap". *International Journal of Mass Spectrometry*, Vol. 358, pp. 1–16, 2014.

[Keysa] Keysight. "33522B Waveform Generator, 30 MHz, 2-Channel with Arb". `https://literature.cdn.keysight.com/litweb/pdf/5992-2572EN.pdf?id=2937598`. Accessed: Jul, 2018.

[Keysb] Keysight. "34470A Digital Multimeter, 7 ½ Digit, Truevolt DMM". `https://literature.cdn.keysight.com/litweb/pdf/5991-1983EN.pdf?id=2318052`. Accessed: Jul, 2018.

[Krem 10] J. Krempel. *A new spectrometer to measure the molar Planck constant.* PhD thesis, Ludwig-Maximilians-Universität München, 2010.

[Kön 19] C. König. *in preparation.* Master's thesis, Ruprecht-Karls-Universität Heidelberg, 2019.

[Line] Linear-Technologies. "LTZ1000 ultra-stable temperature controllable reference". `https://www.analog.com/media/en/technical-documentation/data-sheets/LTZ1000.pdf`. Accessed: Jun, 2019.

[MKS a] MKS-Instruments. "120AD differential pressure sensor". `https://www.mksinst.com/mam/celum/celum_assets/resources/120dif.pdf?1`.

[MKS b] MKS-Instruments. "PR4000B Digital Power Supply and Display". `https://www.mksinst.com/f/pr4000b-digital-power-supply`. Accessed: May, 2019.

[Mukh 08] M. Mukherjee *et al.* "ISOLTRAP: An on-line Penning trap for mass spectrometry on short-lived nuclides". *The European Physical Journal A*, Vol. 35, No. 1, pp. 1–29, Jan 2008.

[NNDC] NNDC. "National Nuclear Data Center NuDat 2.7". `https://www.nndc.bnl.gov/nudat2/reCenter.jsp?z=17&n=18`. Accessed: Jun, 2019.

[NOAA] NOAA. "World magnetic model (WMM) calculated by the National Geospatial-Intelligence Agency". `https://www.ngdc.noaa.gov/geomag/WMM/calculators.shtml`. Accessed: Jan, 2019.

[Rain 04] S. Rainville, J. K Thompson, and D. Pritchard. "An Ion Balance for Ultra-High-Precision Atomic Mass Measurements". *Science (New York, N.Y.)*, Vol. 303, pp. 334–8, 02 2004.

[Rain 05] S. Rainville *et al.* "A direct test of $E = mc^2$". *Nature*, Vol. 438, p. 1096–1097, Dec 2005.

[Repp 12] J. Repp *et al.* "PENTATRAP: a novel cryogenic multi-Penning-trap experiment for high-precision mass measurements on highly charged ions". *Applied Physics B*, Vol. 107, No. 4, pp. 983–996, Jun 2012.

[Repp 15] J. Repp. *The setup of the high-precision Penning-trap mass spectrometer PENTATRAP and first production studies of highly charged ions.* PhD thesis, Ruprecht-Karls-Universität Heidelberg, 2015.

[Risc 11] A. Rischka. "Aufbau und Charakterisierung eines Systems zur Stabilisierung des Magnetfeldes an PENTATRAP". Bachelor's thesis, Ruprecht-Karls-Universität Heidelberg, 2011.

[Risc 14] A. Rischka. *Aufbau des Stabilisierungssystems des Heliumdrucks und Heliumlevels und Konstruktion eines kryogenen Faraday-Bechers für PENTATRAP.* Master's thesis, Ruprecht-Karls-Universität Heidelberg, 2014.

[Risc 18] A. Rischka. *The First Direct Q_{EC} Measurement in ^{163}Ho and the Development of the High-Precision Mass Spectrometer PENTATRAP for Neutrino Physics.* PhD thesis, Ruprecht-Karls-Universität Heidelberg, 2018.

[Roux 12] C. Roux. *High-Resolution Mass Spectrometry: The Trap Design and Detection System of PENTATRAP and New Q-Values for Neutrino Studies.* PhD thesis, Ruprecht-Karls-Universität Heidelberg, 2012.

[Schm 85] U. Schmucker. "Components of the field, units; in Landolt-Börnstein-Group V Geophysics". *Springer*, Vol. B, p. 31 ff., 1985.

[Schu] R. X. Schüßler. *in preparation.* PhD thesis, Ruprecht-Karls-Universität Heidelberg.

[Schw 17] C. Schweiger. *Construction and commissioning of a room-temperature electron beam ion trap and development of a wire probe injection system.* Master's thesis, Ruprecht-Karls-Universität Heidelberg, 2017.

[Siem 10] Siemens. "Funktionsbeschreibung, Projekt: Max-Planck-Institut, Heidelberg Gebäude 16 UG, Neuer Experimentierbereich: PENTATRAP". 2010.

[Simo 92] N. Simon, E. Drexler, and R. Reed. "Properties of copper and copper alloys at cryogenic temperatures. Final report". *Natl. Inst. Stand. Technol. Mono.*, Vol. 177, 2 1992.

[Stef] Stefan-Mayer-Instruments. "Fluxgate magnetic field sensor FL1-100". `https://stefan-mayer.com/images/datasheets/Data-sheet_FL1-100.pdf`. Accessed: Jun, 2018.

[Stre 14] S. Streubel. *Kontrolle der Umwelteinflüsse auf THe-Trap am Beispiel der Bestimmung des Massenverhältnisses von Kohlenstoff-12 zu Sauerstoff-16.* PhD thesis, Ruprecht-Karls-Universität Heidelberg, 2014.

[Toel] Toellner. "Multiple-output power supply 8733". `https://www.toellner.de/datenblaetter/de_8732_8735.pdf`. Accessed: Jul, 2018.

[Van 99] R. S. Van Dyck, D. L. Farnham, S. L. Zafonte, and P. B. Schwinberg. "Ultrastable superconducting magnet system for a penning trap mass spectrometer". *Review of Scientific Instruments*, Vol. 70, No. 3, pp. 1665–1671, 1999.

[Vari 15] Varian. "7-T superconducting magnet". personal communication, 2015.

[VRN] VRN. "VRN Heidelberg tram route timetables". `https://www.vrn.de/mng/#/XSLT_TRIP_REQUEST2@init`. Accessed: Apr, 2019.

[Wine 75] D. J. Wineland and H. G. Dehmelt. "Principles of the stored ion calorimeter". *Journal of Applied Physics*, Vol. 46, No. 2, pp. 919–930, 1975.

Danksagung

Mein besonderer Dank geht an dieser Stelle an alle, die mich während meiner Masterarbeit unterstützt haben.

Zu allererst geht mein Dank an Klaus Blaum. Vielen Dank für die Aufnahme in diese tolle Abteilung und das Ermöglichen bei einer so spannenden Forschung mitzuwirken. Deine gute Laune, volle Unterstützung und die Zeit und den Aufwand den du in die exzellente Betreuung von jedem Einzelnen steckst, haben ein einmaliges Arbeitsumfeld geschaffen.

Vielen Dank an Wolfgang Quint für seine selbstverständliche Bereitschaft das Zweitgutachten meiner Arbeit zu erstellen.

An Menno Door und Alexander Rischka für meine Betreuung und das Korrekturlesen meiner Arbeit. An Menno für die tolle Hilfe im Labor, am PC und das gelegentliche Leihen deiner funktionierenden Beine. Besonderen Dank dafür, dass du gegen Ende nicht die Geduld mit mir verloren hast und keine noch so langwierige Diskussion gescheut hast. An Alex, vielen Dank für die Betreuung der ersten Hälfte meiner Masterarbeit und die vielen Hilfen im Labor, beim Programmieren und bei der Datenanalyse.

Vielen Dank an die beste Büronachbarin die man sich vorstellen kann, Rima Schüßler, für dein allzeit offenes Ohr, wundervolle Unterhaltungen, niemals Langeweile, entspannte Kaffeepausen, präziseste Korrekturen und mein persönliches Büro-google for all things PENTATRAP.

Vielen Dank an das ganze PENTATRAP team Sergey Eliseev, Christoph Schweiger, Charlotte König, Pavel Filianin, Daniel Lange und Wenjia Huang für die Unterstützung, tolle Zusammenarbeit und viele unterhaltsame Stunden auch außerhalb des Instituts. Insbesondere geht mein Dank an Sergey für die intensive Ionenarbeit und Datenaufnahme, sodass es während meiner Masterarbeit nie einen Mangel an Messdaten gab. Vielen Dank auch an Christoph für die musikalische Untermalung meiner Masterzeit.

Vielen Dank an Ralph Zilly, für die Unterstützung im technischen Bereich.

Thanks to all the fellow Penning trappers from ALPHATRAP and THe-TRAP for the great lunches and fascinating conversations. The scientific exchange that you offer, will never be taken for granted.

Ein ganz besonderer Dank geht auch an meine ganze Familie. An Ursula Kromer für ihre Geduld, unfassbare Unterstützung die immer nur ein Anruf entfernt war und für die sprachlichen Korrekturen dieser Arbeit. An Thomas Kromer dafür dass du mir immer den Rücken frei hälst. Vielen Dank an beide meine Eltern auch für die großartige Hilfe nach meinen Knie-OPs, dank euch war ich schnell wieder auf den Beinen und konnte die Masterarbeit fortführen. An Christian und Daniela Kromer die dafür sorgen, dass Familientreffen nie langweilig werden und die mein top aufgestelltes Team für last minute Krisensitzungen sind.

Erklärung

Ich versichere, dass ich diese Arbeit selbstständig verfasst und keine anderen als die angegebenen Quellen und Hilfsmittel benutzt habe.

Heidelberg, den 1.7.2019